ORIGINAL ARTICLE



Lipid biomarkers recording marine microbial community structure changes through the Frasnian-Famennian mass extinction event

Jian Chen¹ | Nicholas Hogancamp² | Man Lu¹ | Takehito Ikejiri^{1,3} | Natalia Malina⁴ | Ann Ojeda⁴ | YongGe Sun⁵ | YueHan Lu¹ ©

¹Molecular Eco-Geochemistry (MEG) Laboratory, Department of Geological Sciences. The University of Alabama. Tuscaloosa, Alabama, USA

²Department of Earth and Atmospheric Sciences, University of Houston, Houston,

³Alabama Museum of Natural History, The University of Alabama, Auburn, Alabama, USA

⁴Department of Geosciences, Auburn University, Tuscaloosa, Alabama, USA

⁵Organic Geochemistry Unit, Key Laboratory of Geoscience Big Data and Deep Resource of Zhejiang Province, School of Earth Sciences, Zhejiang University, Hangzhou, China

Correspondence

YueHan Lu, Molecular Eco-Geochemistry (MEG) Laboratory, Department of Geological Sciences, The University of Alabama, Tuscaloosa, AL 35485, USA. Email: yuehan.lu@ua.edu

YongGe Sun, Organic Geochemistry Unit, Key Laboratory of Geoscience Big Data and Deep Resource of Zhejiang Province, School of Earth Sciences, Zhejiang University, Hangzhou 310027, China. Email: ygsun@zju.edu.cn

Funding information

American Association of Petroleum Geologists Foundation: American Chemical Society, Grant/Award Number: PRF#61366-ND2; Gulf Coast Association of Geological Societies; Geological Society of America

[Correction added on 02 Aug 2023, after first online publication: The isothermal hold time for 220°C (2 minutes) has been added to section 3.3 in this updated version of the article.]

Abstract

Studying the response and recovery of marine microbial communities during mass extinction events provides an evolutionary window through which to understand the adaptation and resilience of the marine ecosystem in the face of significant environmental disturbances. The goal of this study is to reconstruct changes in the marine microbial community structure through the Late Devonian Frasnian-Famennian (F-F) transition. We performed a multiproxy investigation on a drill core of the Upper Devonian New Albany Shale from the Illinois Basin (western Kentucky, USA). Aryl isoprenoids show green sulfur bacteria expansion and associated photic zone euxinia (PZE) enhancement during the F-F interval. These changes can be attributed to augmented terrigenous influxes, as recorded collectively by the long-chain/shortchain normal alkane ratio, carbon preference index, C₃₀ moretane/C₃₀ hopane, and diahopane index. Hopane/sterane ratios reveal a more pronounced dominance of eukaryotic over prokaryotic production during the mass extinction interval. Sterane distributions indicate that the microalgal community was primarily composed of green algae clades, and their dominance became more pronounced during the F-F interval and continued to rise in the subsequent periods. The 2α -methylhopane index values do not show an evident shift during the mass extinction interval, whereas the 3βmethylhopane index values record a greater abundance of methanotrophic bacteria during the extinction interval, suggesting enhanced methane cycling due to intensified oxygen depletion. Overall, the Illinois Basin during the F-F extinction experienced heightened algal productivity due to intensified terrigenous influxes, exhibiting similarities to contemporary coastal oceans that are currently undergoing globalized cultural eutrophication. The observed microbial community shifts associated with the F-F environmental disturbances were largely restricted to the extinction interval, which suggests a relatively stable, resilient marine microbial ecosystem during the Late Devonian.

KEYWORDS

cyanobacteria, Devonian, euxinia, Kellwasser Event, lipid biomarker, methanotroph

1 | INTRODUCTION

Microbial communities constitute the base of most marine food webs and contribute to essential marine ecosystem functions (Azam & Malfatti, 2007). The response of marine microbes to changing environmental conditions on a geological time scale, especially those associated with catastrophic mass extinction events, provides an evolutionary window through which to understand the adaptation and resilience of the marine ecosystem in the face of significant environmental changes (Cao et al., 2009; Fox et al., 2020; Kasprak et al., 2015; Richoz et al., 2012; Rohrssen et al., 2013; Sepulveda et al., 2009; Smolarek et al., 2017; Xie et al., 2007; Xie et al., 2010; Xie et al., 2017). Previous studies have reported various types and levels of responses (or no response) of marine microbes to the Phanerozoic mass extinction events (Richoz et al., 2012; Rohrssen et al., 2013; Sepulveda et al., 2009; Xie et al., 2007). More research, however, is needed to better understand the spatial scale (whether regional, continental, or global) and diverse forms of these responses, as well as environmental factors modulating marine microbial responses and leading to their diversification or demise.

Fossil lipid biomarkers are a powerful tool to investigate changes in the marine microbial community structure in response to catastrophic disturbances during Phanerozoic mass extinction events (Schwark & Empt, 2006; Xie et al., 2005). Relative to the conventional paleontological approach relying on body fossils, lipid biomarkers offer advantages in quantitatively recording biomass and activities of microbes that lack hard parts (e.g., teeth, bones). For example, Rohrssen et al. (2013), based on major shifts in biomarker distributions across the Late Ordovician-Early Silurian boundary in North America, suggested that the contributions of bacteria, especially methanotrophic bacteria, increased during warm intervals of the Late Ordovician Hirnantian glaciation. Xie et al. (2005, 2007) reported two episodes of cyanobacterial blooms near the Permian-Triassic boundary, based on biomarker evidence from the Meishan section in South China. Sepulveda et al. (2009), using biomarker assemblages from the Cretaceous-Paleogene boundary layer in Denmark, revealed that algal productivity decreased briefly before a rapid resurgence and ecological reorganization.

The objective of this study is to reconstruct changes in the marine microbial community structure through the Late Devonian Frasnian-Famennian (F-F) mass extinction. The F-F biotic crisis was marked by a succession of extinction pulses, with the most significant one recorded in shallow-marine ecosystems during the Upper Kellwasser (UKW) event (House, 2002). The extrinsic causal mechanism for the mass extinction remains a topic of ongoing debate, with rapid afforestation, volcanism, global cooling, and transgression among the most speculated triggers (Algeo et al., 1995; Bond & Wignall, 2008; Joachimski & Buggisch, 2002; Lu et al., 2019; Racki et al., 2018). Ongoing discussion also continues around the

direct kill mechanism, bringing forward multiple hypotheses such as sulfide poisoning (Chen et al., 2013) and ocean acidification (Kabanov et al., 2023; Zeng et al., 2011). However, there is a broad consensus that the Late Devonian marine environment is overall reducing, leading to prolonged oxygen stress that is considered to be a significant contributing factor to taxonomic and ecological turnovers of marine organisms (Boyer et al., 2021; Carmichael et al., 2019; Lu, Lu, Ikejiri, Sun, et al., 2021). Oxygen scarcity and stress in marine environments not only is a feature shared by multiple mass extinction events (e.g., Late Devonian, Permian-Triassic, and end-Triassic; Cao et al., 2009; Carmichael et al., 2019; Kasprak et al., 2015) but also represents a likely future scenario of modern coastal oceans experiencing globalized cultural eutrophication (Diaz et al., 2004; Diaz & Rosenberg, 2008; Malone & Newton, 2020). Therefore, studying the response of the marine microbial community during the Late Devonian mass extinction allows constraining and predicting how widespread oceanic anoxia can shape the evolutionary trajectory of marine microbial ecosystems, when the differences in the rates and scales between geological events and anthropogenic effects are properly taken into account.

Here, we present multiproxy geochemical evidence for the community-level response and recovery of marine microbes associated with environmental disturbances during the Late Devonian F-F mass extinction. Through analyzing a suite of organic geochemical proxies on a drill core of the Upper Devonian New Albany Shale, we reconstruct changes in the marine microbial community and contemporaneous paleoenvironmental conditions in a tropical-subtropical epicontinental oceanic basin. The study section spans from the lower Frasnian to the middle Famennian, including pre-, intra-, and post-F-F mass extinction intervals, which allows for studying both the response and recovery at the community level. Our results offer new insights into how severe environmental disturbances can shape marine microbial ecosystems, which sheds light on the resilience of oceans in the face of environmental degradation and climate change.

2 | GEOLOGICAL SETTING

2.1 | Late Devonian paleogeography

The Illinois Basin, located in southern Euramerica during the Late Devonian, is part of the epicontinental seas that inundated the North American craton (Figure 1(a); Algeo & Tribovillard, 2009). Situated approximately from 30S° paleolatitude to the paleoequator, the basin was connected to the Rheic Ocean through the Cumberland Sill (Song et al., 2021) and bounded by a series of uplifts and highlands (e.g., the Acadian Orogen, the Cincinnati Arch, the Nashville Dome) that were produced by orogenic processes associated with the collision between Euramerica and Gondwanaland (Figure 1(b); Algeo & Tribovillard, 2009).

FIGURE 1 Paleogeography and study site. (a) Late Devonian global paleogeography (ca. 370 Ma; Golonka 2020); (b) the Illinois Basin in Euramerica (Song et al., 2021); (c) subsurface and outcrop distributions of the New Albany Shale (Mastalerz et al., 2013) and the locations of study core T-6590 (this study) and core BCC (Over et al., 2019). Panel (b) is an enlarged view of the red rectangle in panel (a) that outlines the Illinois and Appalachian Basins on the North American Craton.

2.2 | Lithostratigraphy and biostratigraphy of the New Albany Shale

The Middle-Late Devonian New Albany Shale of the Illinois Basin is widely distributed in Kentucky, Indiana, and Illinois (Figure 1(c)). Stratigraphically, the New Albany Shale correlates with the Ohio Shale, Chattanooga Shale, Woodford Shale, and Antrim Shale in the central and eastern United States. The study section is a drill core (T-6590) recovered from well SA-005, McLean County, western Kentucky (N 37.42°, W 87.28°) (Figure 1(c)). In the core T-6590, the New Albany Shale is approximately 83 m thick, underlain by the

Middle Devonian Sellersburg Limestone and overlain by the Lower Mississippian Hannibal Shale. The New Albany Shale consists of five members—the Blocher, Selmier, Morgan Trail, Camp Run, and Clegg Creek in ascending order (Figure 2). Detailed lithological descriptions can be found in Supplementary Material S1.

Biostratigraphic ages were assigned to each member of the New Albany Shale by collecting conodonts from bedding planes of the T-6590 core and comparing the results to published conodont results from nearby localities (Over et al., 2019). More information on the New Albany Shale biostratigraphy can be found in Supplementary Material S2 and Figures S1–S5.

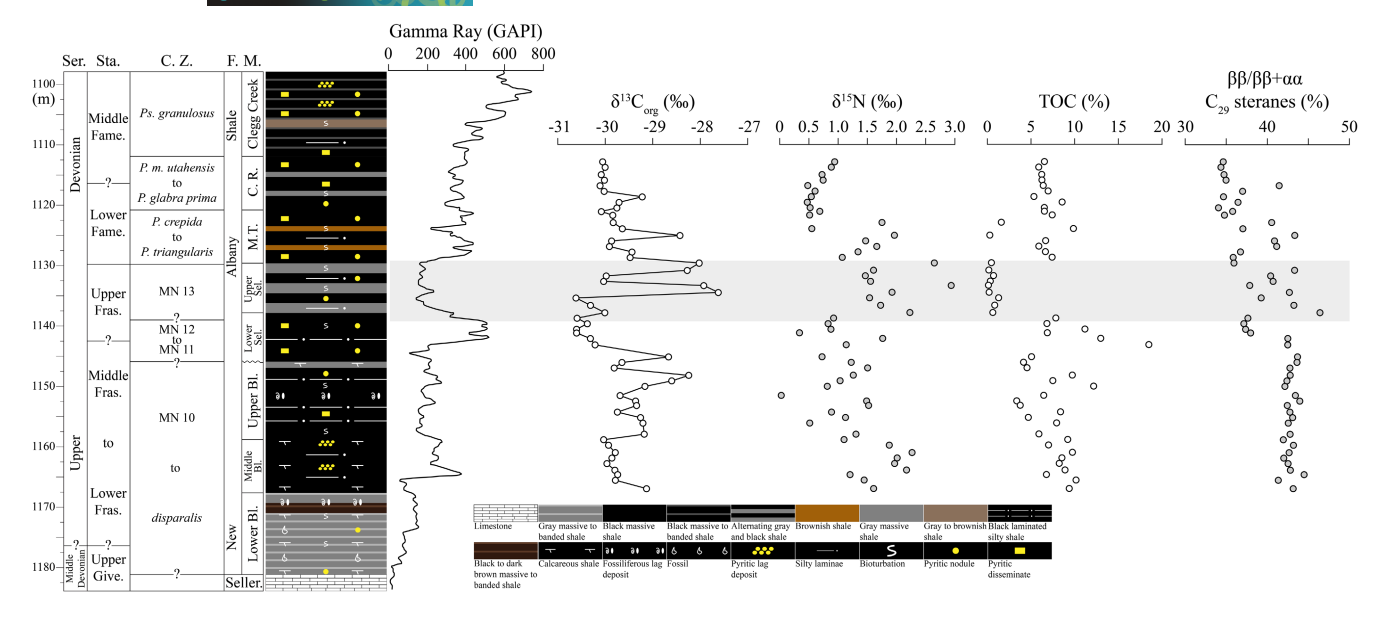


FIGURE 2 Middle-Late Devonian lithostratigraphy, biostratigraphy, and chemostratigraphy of core T-6590. Biostratigraphy is based on conodont examination in the study core T-6590 following conodont zonation defined by previous studies (Over et al., 2019). The gray area highlights the F-F mass extinction interval. Abbreviations: Bl.—Blocher; C.R.—Camp Run; C.Z.—conodont zonation; F.—Formation; Fame.—Famennian; Fras.—Frasnian; Give.—Givetian; m.—marginifera; M.—Member; M.T.—Morgan Trail; P.—Palmatolepis; Ps.—Pseudopolygnathus; Sel.—Selmier; Seller.—Sellersburg; Ser.—Series; Sta.—Stage.

2.3 | Frasnian-Famennian mass extinction interval identification

The Late Devonian F-F mass extinction event (i.e., Kellwasser Event) is known for its dramatic impacts on tropical marine fauna. The F-F event is identified as two biotic events, the LKW and UKW events, but the two events cannot be always differentiated (Carmichael et al., 2019). The identification of the F-F mass extinction interval in the study section is based on combined evidence of lithostratigraphy, biostratigraphy, and geochemistry. Following previous investigations of outcrops and cores of the New Albany Shale (Over et al., 2019), we placed the F-F boundary near the Selmier-Morgan Trail boundary. The position of the boundary is supported by the conodont data of the study core (Supplementary Material S2, Figures S1-S5). Previous studies show that UKW is within the conodont MN zones 13b to 13c and right below the F-F boundary, and LKW correlates with the Upper MN Zone 12 and is immediately below the MN 12-13 boundary (Day & Witzke, 2017). Also, positive excursions in δ^{13} C of organic carbon (δ^{13} C_{org}) have been used as a chemostratigraphic marker for the Kellwasser events, despite variable shapes and amplitudes of the excursions have been reported globally (Carmichael et al., 2019; Day & Witzke, 2017). The correlation of multiple closely spaced $\delta^{13}C$ excursions with UKW has been previously observed in some localities (Hillbun et al., 2015; Whalen et al., 2015). In the study core, the two closely spaced, positive $\delta^{13} \text{C}_{\text{org}}$ excursions (+2.7% and +1.7% relative to the average of the uppermost value and lowermost value of the identified F-F interval) in the MN Zone 13-P. triangularis Zone were used as a geochemical marker for the UKW event (Figure 2). The LKW event, however, was not identified, as the

conodont data cannot determine the exact location of the boundary between the MN Zone 13 and MN Zone 12 (Supplementary Material S2 & Figures S1–S5). Also, there is no evident $\delta^{13}C_{org}$ excursion near the possible stratigraphic position. Thus, the F-F mass extinction interval was placed within the MN Zone 13 in the study core (Figure 2).

3 | MATERIALS AND METHODS

3.1 | Samples

A total of 55 samples were collected to analyze bulk organic geochemical parameters and lipid biomarkers from the T-6590 drill core of the New Albany Shale. The core was recovered in 2010 and has since been curated at the Earth Analysis Research Library (EARL) of the Kentucky Geological Survey (KGS). Samples were collected in the core depth of 1110–1170m at a nearly constant interval of approximately 1 m. Before laboratory analyses, samples were washed using deionized, ultrapure carbon-free water and dichloromethane to remove potential contaminants on the core surface. Cleaned samples were then ground into a 100–200 mesh powder.

3.2 | Bulk organic geochemical analyses

Six samples were submitted to the Source Rock Lab, GeoMark Research Inc. to determine the thermal maturity parameter of organic matter, $T_{\rm max}$. All 55 samples were analyzed for total organic

gebiology WILEY 5

carbon (TOC), $\delta^{13}C_{org}$, and bulk $\delta^{15}N$. Detailed information on the analytical method and associated accuracy and precision are presented in Supplementary Material S3.1 and S3.2.

3.3 | Biomarker and compound-specific carbon isotopic analyses

Cleaned powdered samples (approximately 18–32 g, depending on the level of TOC) were Soxhlet extracted with dichloromethane and methanol (97:3, v:v) at 48°C for 72 h. Acid-pretreated copper slices were ultrasonically cleaned in dichloromethane and methanol (97:3, v:v) before they were added to the Soxhlet extracts to remove elemental sulfur. Deuterated n-tetracosane ($C_{24}D_{50}$) was added to the extracts for normal alkane quantification. After removing asphaltenes via precipitation, the extracts were loaded into a column filled with 60–100 mesh activated (pre-baked at 150°C for 4h) silica gel and 100–200 mesh activated (pre-baked at 450°C for 4h) alumina (silica gel: alumina=3:1 by volume). Aliphatic, aromatic, and polar fractions were eluted successively by petroleum ether, benzene, and methanol, respectively.

The aliphatic and aromatic fractions were further analyzed on an Agilent 7890B gas chromatography (GC)-5977A mass spectrometer (MS). Prior to the instrumental analysis, known amounts of $5\beta(H)$ cholane $(C_{24}H_{42})$ and C_{30} $17\beta(H)$, $21\beta(H)$ hopane $(C_{30}H_{52})$ (Chiron AS) were added to the aliphatic fraction for quantifying sterane and hopane biomarkers, respectively. Deuterated phenanthrene (C₁₄D₁₀) was added to the aromatic fraction for quantifying aromatic biomarkers. The GC-MS was equipped with a DB-1MS capillary column ($60 \,\mathrm{m} \times 0.32 \,\mathrm{mm} \times 0.25 \,\mu\mathrm{m}$ film thickness), with the carrier gas (helium) flow set at 1.0 mL/min. For both aliphatic and aromatic fractions, the initial GC oven temperature was 80°C with an isothermal hold for 2 min, increased at 3°C /min to 220°C, isothermally held for 2 min, and then at 2°C /min to 300°C, where it was held for 30 min. The electron ionization (EI) source was operated at 70 eV and 230°C. All hydrocarbons were analyzed at the full scan mode, and the aliphatic fraction was also analyzed at the selected ion monitoring (SIM) mode for hopanes (m/z=191) and steranes (m/z=217). Compounds were quantified from their peak areas relative to the peak area of the internal standards.

To identify and quantify methylhopanes, aliphatic hydrocarbons were further analyzed on an Agilent 7890B gas chromatography-7000C triple quadrupole–mass spectrometer (GC-QQQ-MS) in the multiple reaction monitoring mode. The GC-QQQ-MS was equipped with a DB-EUPAH column ($60m\times250\mu m\times0.25\mu m$ film thickness) and a restrictor ($0.7m\times150\mu m$). The carrier gas flow of helium was set at 1.5mL/min for the DB-EUPAH column and was set at 3.34mL/min for the restrictor. The quench gas (helium) flow was 2.25mL/min, and the collision gas (nitrogen) flow was 1.5mL/min. The GC oven temperature program was initially set at 60°C with an isothermal hold of 2min, ramped up at 8°C /min to 220°C, and then at 2°C/min to 325°C, where it was held for 20.5min. The EI source was

operated at 70 eV and 230 °C, and the quadrupole was operated at 150 °C.

3.4 | Compound-specific carbon isotopic analyses

Aliphatic and aromatic hydrocarbons of two selected samples (before and during the extinction interval, respectively) were analyzed for compound-specific δ^{13} C values. Prior to the analysis, the aromatic fraction was further separated and purified following the method detailed by (Jiang et al., 2013). The fraction was loaded into a column (6cm length, 6 mm internal diameter) filled with 100–200 mesh activated (pre-baked at 450°C for 4h) alumina. Subfractions 1, 2, and 3 were eluted successively using petroleum ether and DCM (99:1, v:v), petroleum ether and DCM (97:3, v:v), and DCM, respectively.

To analyze δ^{13} C of short-chain n-alkanes and aryl isoprenoids, the aliphatic fraction and aromatic subfraction 1 were further analyzed on a gas chromatograph Trace 1310 coupled to a Delta V isotope ratio mass spectrometer (GC-IRMS). The GC-IRMS is equipped with a TG-5 ms column ($30\,\text{m}\times250\,\mu\text{m}\times0.25\,\mu\text{m}$ film thickness). The initial GC oven temperature was at 80° C with an isothermal hold of 5 min, increased to 220° C at 5° C/min followed by an isothermal hold of 2 min, and then ramped up to 300° C at 5° C/min with an isothermal hold of 5 min. Helium was used as a carrier gas at a flow rate of 1 mL/min. Each sample was measured in duplicate, and the mean and standard deviation δ^{13} C values are reported in ‰ relative to V-PDB.

4 | RESULTS

4.1 Bulk organic geochemistry

 $T_{\rm max}$ values vary in a narrow range of 438–448°C, which corresponds to calculated vitrinite reflectance (Ro) values in the range of 0.72–0.90. This range is similar to what was observed for the Late Devonian section in the Appalachian Basin, 440–444°C (Haddad et al., 2016). These values indicate that the thermal maturity of organic matter is in the early to peak stage of the oil generation window (Peters et al., 2005). The thermal maturity parameters of extractable organic matter, $\beta\beta/(\beta\beta+\alpha\alpha)$ C₂₉ sterane (34.05%–46.42%; Figure 2), also fall within the range for the early to peak stage of the oil generation window (Peters et al., 2005), suggesting that extractable organic matter has not been affected by migration. TOC values fluctuate in a wide range of 0.11% to 18.50%, δ^{13} Corg values vary from -30.6% to -27.6‰, and δ^{15} N values vary from 0.03‰ to 2.94‰ (Figure 2).

4.2 | Biomarkers

The carbon number of detected normal alkanes ranges from $\rm C_{13}$ to $\rm C_{31}$, and low-molecule-weight homologs ($\rm C_{14}$ to $\rm C_{21}$) are

TABLE 1 Statistical average and standard deviation of geochemical parameters of the study core of New Albany Shale.

Parameters	Pre-F-F interval	F-F interval	Post-F-F Interval	Whole section
TOC (%)	8.06 ± 3.26	1.25 ± 2.34	6.16 ± 2.18	6.20 ± 3.71
$\delta^{13}C_{\text{org}}$ (‰)	-29.63 ± 0.58	-29.34 ± 1.22	-29.75 ± 0.42	-29.62 ± 0.70
δ ¹⁵ N (‰)	1.26 ± 0.55	1.86 ± 0.60	0.94 ± 0.49	1.26 ± 0.62
$n-C_{15,17,19}$ alkanes (µg/g TOC)	213.54 ± 64.58	347.95 ± 220.00	193.02 ± 94.63	231.26 ± 126.73
Aryl isoprenoids (μg/g TOC)	30.51 ± 14.98	54.94 ± 31.27	42.86 ± 17.88	38.99 ± 21.44
AIR	2.44 ± 0.99	0.79 ± 0.63	1.92 ± 1.01	1.97 ± 1.11
TAR	0.16 ± 0.08	0.22 ± 0.14	0.13 ± 0.07	0.16 ± 0.09
CPI	1.06 ± 0.03	1.11 ± 0.11	1.05 ± 0.05	1.07 ± 0.06
C ₃₀ moretane/C ₃₀ hopane	0.11 ± 0.01	0.13 ± 0.03	0.12 ± 0.03	0.12 ± 0.02
C ₃₀ dihopane index (%)	13.17 ± 2.26	14.45 ± 3.72	12.35 ± 0.80	13.14 ± 2.34
C ₃₃₋₃₅ HHI (%)	31.45 ± 1.90	38.39 ± 3.34	33.46 ± 5.65	33.37 ± 4.49
Hopane/sterane	0.70 ± 0.12	0.40 ± 0.11	0.61 ± 0.14	0.62 ± 0.16
%C ₂₇ sterane (%)	32.55 ± 1.28	32.09 ± 1.58	30.70 ± 1.63	31.86 ± 1.65
%C ₂₈₊₂₉ sterane (%)	67.45 ± 1.28	67.91 ± 1.58	69.30 ± 1.63	68.14 ± 1.65
C ₂₈ /C ₂₉ sterane	0.61 ± 0.04	0.53 ± 0.06	0.59 ± 0.04	0.59 ± 0.05
2α-MHI (%)	2.07 ± 0.37	1.43 ± 1.27	1.73 ± 0.69	1.84 ± 0.74
3β-MHI (%)	1.71 ± 0.28	2.28 ± 1.11	1.62 ± 0.74	1.78 ± 0.69

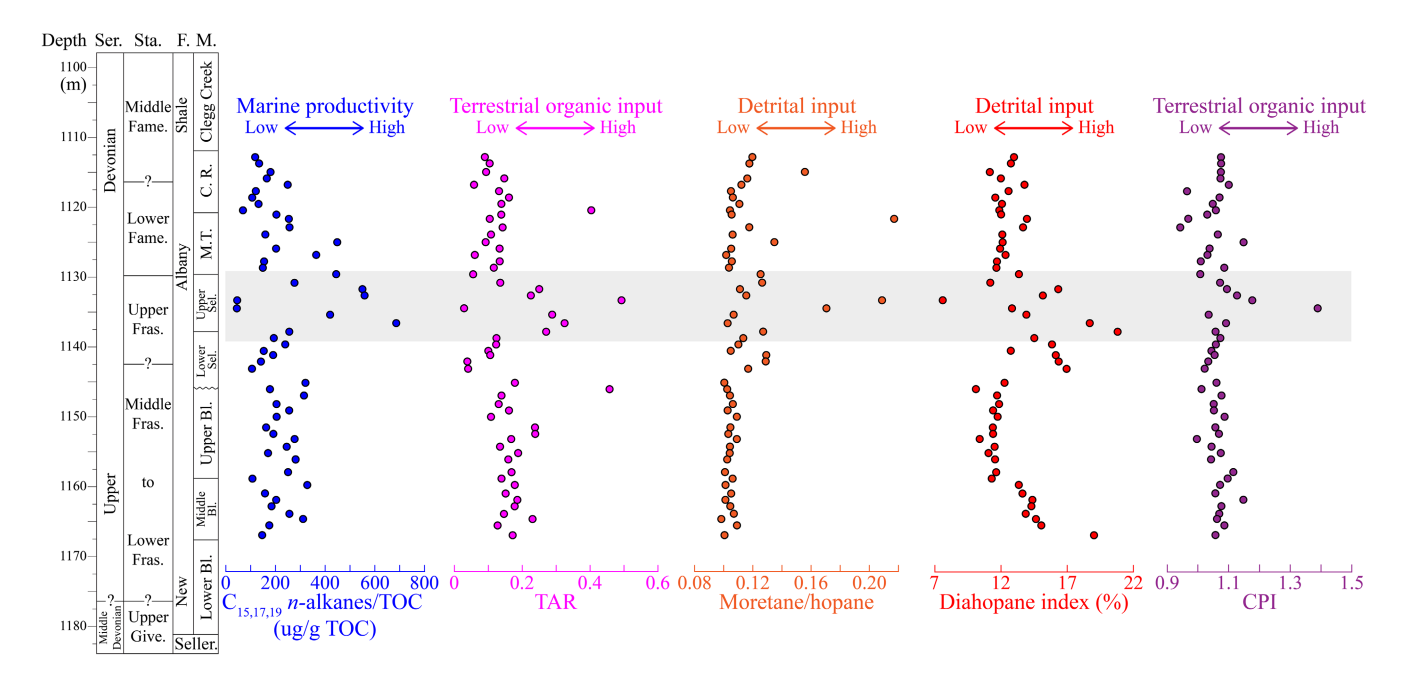


FIGURE 3 Biomarker stratigraphic profiles of the Upper Devonian New Albany Shale from the Illinois Basin (core T-6590). $C_{15,17,19}$ n-alkanes/TOC-concentrations of $C_{15,17,19}$ n-alkanes relative to TOC; TAR-terrestrial/aquatic ratio: concentration ratio of long-chain ($C_{27,29,31}$) to short-chain ($C_{15,17,19}$) n-alkanes; C_{30} Moretane/ C_{30} hopane: concentration ratio of C_{30} $\beta \alpha$ hopane to C_{30} $\alpha \beta$ hopane; diahopane index: concentration ratio of C_{30} 17α (H)-diahopane and C_{30} $\alpha \beta$ hopane; CPI-Carbon Preference Index= $0.5 \times (C_{25} + C_{27} + C_{29} + C_{31} + C_{33}) \times [1/(C_{24} + C_{26} + C_{28} + C_{30} + C_{32}) + 1/(C_{26} + C_{28} + C_{30} + C_{32} + C_{34})]$. The gray area highlights the F-F mass extinction interval. Bl.—Blocher; C.R.—Camp Run; F.—Formation; Fame.—Famennian; Fras.—Frasnian; Give.—Givetian; M.—Member; M.T.—Morgan Trail; Sel.—Sellier; Seller.—Sellersburg; Ser.—Series; Sta.—Stage

more abundant (Figure S6). The concentrations of $n\text{-C}_{15,17,19}$ alkanes/TOC are higher and more variable during the F-F interval (347.95 \pm 220.00 μ g/gTOC)thanthose before and after the extinction interval (213.54 \pm 64.58 μ g/g TOC and 193.02 \pm 94.63 μ g/g TOC,

respectively; Table 1; Figure 3). The terrestrial/aquatic ratio (TAR) is calculated as the ratio of the concentration of long-chain n-alkanes ($C_{27,29,31}$) to those of short-chain n-alkanes ($C_{15,17,19}$). TARs are overall higher and more fluctuating during the F-F interval

(0.22 \pm 0.14) than before (0.16 \pm 0.08) and after (0.13 \pm 0.07) the interval. The Carbon Preference Index (CPI) is calculated as 0.5 \times (C $_{25}$ +C $_{27}$ +C $_{29}$ +C $_{31}$ +C $_{33}$)×[1/(C $_{24}$ +C $_{26}$ +C $_{28}$ +C $_{30}$ +C $_{32}$)+1/(C $_{26}$ +C $_{28}$ +C $_{30}$ +C $_{32}$ +C $_{34}$)]. The CPI values range between 0.94 and 1.39 and are higher during the F-F interval (1.11 \pm 0.11) than those below (1.06 \pm 0.03) and above (1.05 \pm 0.05) the interval (Table 1; Figure 3).

Detected hopanoids include C₂₉ to C₃₅ hopane, C₂₇ norhopane, C₂₇ and C₂₉ norneohopane, and C₃₀ diahopane (Figure S7). C₃₀ moretane/ C_{30} hopane ratios (i.e., C_{30} $\beta\alpha$ hopane/ C_{30} $\alpha\beta$ hopane) exhibit higher values within the F-F mass extinction interval (0.13 \pm 0.03) than the strata below (0.11 ± 0.01) and above (0.12 ± 0.03) the interval (Table 1; Figure 3). The diahopane index was calculated as the ratio of C_{30} 17 α (H)-diahopane/(C_{30} 17 α (H)-diahopane+ C_{30} $\alpha\beta$ hopane), showing higher and more variable values during the F-F interval (14.45% ± 3.72%) compared to those values before and after the interval, which are $13.17\% \pm 2.26\%$ and $12.35\% \pm 0.80\%$, respectively (Table 1; Figure 3). C₃₃₋₃₅ homohopane index (C₃₃₋₃₅ HHI) was calculated as the ratio of C_{33-35} $\alpha\beta$ hopanes to the sum of $\text{C}_{31\text{-}35}~\alpha\beta$ hopanes. $\text{C}_{33\text{-}35}$ HHI values are higher during the mass extinction interval (38.39% \pm 3.34%) in comparison to those before $(31.45\% \pm 1.90\%)$ and after $(33.46\% \pm 5.65\%)$ the interval (Table 1; Figure 4).

Low concentrations of C $_{31}$ 2 α -methylhopanes and C $_{31}$ 3 β -methylhopane are detected (Figure S8). C $_{31}$ 2 α -methylhopane

index (2 α -MHI) is calculated as C $_{31}$ 2 α -methylhopanes/(C $_{31}$ 2 α -methylhopanes+C $_{30}$ $\alpha\beta$ hopane), and C $_{31}$ 3 β -methylhopane index (3 β -MHI) is calculated as C $_{31}$ 3 β -methylhopane/(C $_{31}$ 3 β -methylhopane+C $_{30}$ $\alpha\beta$ hopane). The 2 α -MHI values during the mass extinction (1.43% \pm 1.27%) display more pronounced variations and a lower mean than those below (2.07% \pm 0.37%) and above (1.73% \pm 0.69%) the extinction (Table 1; Figure 4). Most zeros (i.e., C $_{31}$ 2 α -methylhopane below detection) fall within the mass extinction interval. 3 β -methylhopane exhibits a higher mean during the mass extinction interval (2.28% \pm 1.11%) than during the strata below (1.71% \pm 0.28%) and above (1.62% \pm 0.74%; Table 1; Figure 4).

A series of 2,3,6-trimethyl aryl isoprenoids of C_{13} to C_{22} are identified, among which C_{14-16} and C_{18-19} are usually the most abundant compounds (Figure S9). Aryl isoprenoid concentrations/TOC are higher and more variable in the F-F interval (54.94 \pm 31.27 µg/g TOC) than in the strata preceding (30.51 \pm 14.98 µg/g TOC) and following (42.86 \pm 17.88 µg/g TOC) the interval (Table 1; Figure 4). Shortchain to intermediate-chain (i.e., C_{13-17}/C_{18-22}) aryl isoprenoid ratios (AIRs) are lower (0.79 \pm 0.63) within the mass extinction interval as compared to those from the pre-extinction (2.44 \pm 0.99) and post-extinction (1.92 \pm 1.01) strata (Table 1; Figure 4).

 C_{27} to C_{29} regular steranes and diasteranes are the most dominant compounds in the sterane series, and steranes of C_{27} , C_{28} , and C_{29} exhibit a V-shaped distribution, i.e., $C_{27} > C_{28} < C_{29}$

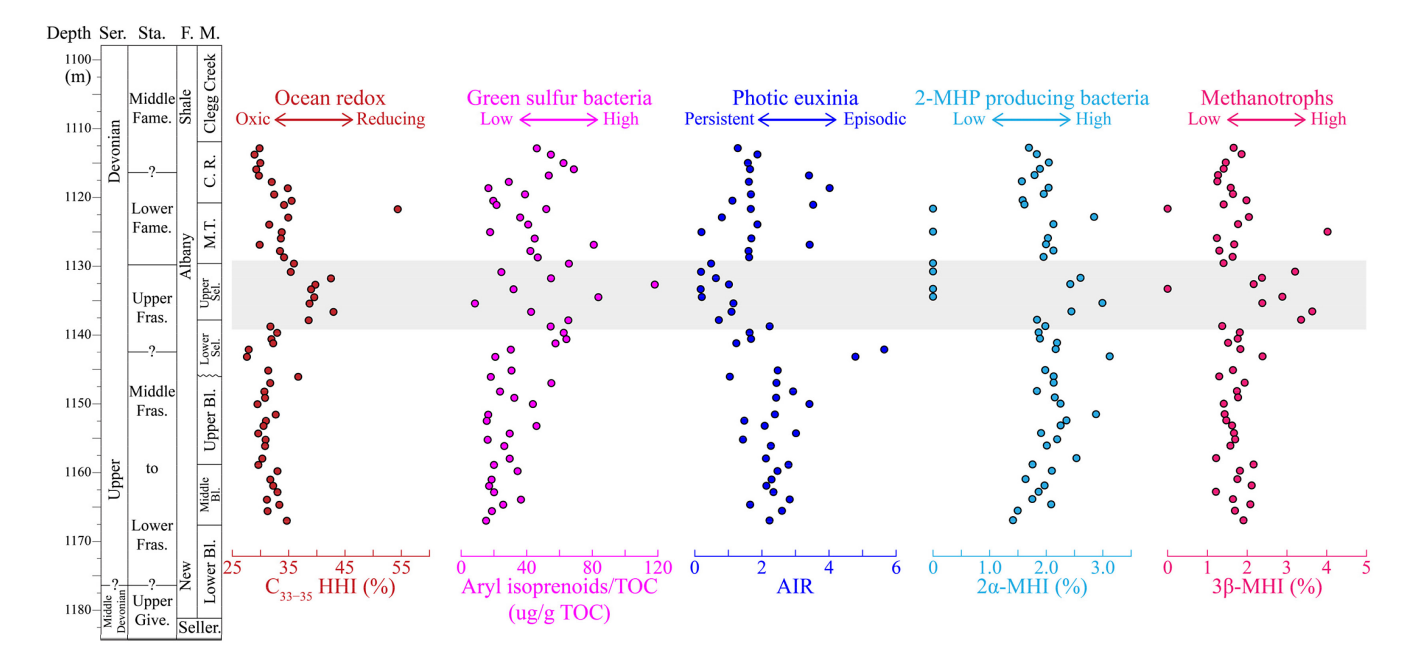


FIGURE 4 Biomarker stratigraphic profiles of the Upper Devonian New Albany Shale from the Illinois Basin (core T-6590). C_{33-35} HHI— C_{33-35} homohopane index: concentration ratio of C_{33-35} $\alpha\beta$ hopanes to C_{31-35} $\alpha\beta$ hopanes. Aryl isoprenoids/TOC: concentrations of C_{13} to C_{22} aryl isoprenoids relative to TOC; AIR—aryl isoprenoid ratio: concentration ratio of short-chain (C_{13-17}) to intermediate-chain (C_{18-22}) aryl isoprenoids; 2α -MHI— C_{31} 2α -methylhopane index = the ratio of C_{31} 2α -methylhopanes to the sum of C_{31} 2α -methylhopane and C_{30} $\alpha\beta$ hopane. 3β -MHI— C_{31} 3β -methylhopane index = the ratio of C_{31} 3β -methylhopane to the sum of C_{31} 3β -methylhopane and C_{30} $\alpha\beta$ hopane. The gray area highlights the F-F mass extinction interval. BI.—Blocher; C.R.—Camp Run; F.—Formation; Fame.—Famennian; Fras.—Frasnian; Give.—Givetian; M.—Member; M.T.—Morgan Trail; Sel.—Sellers-Sellers-Sellers-Sellers-Series; Sta.—Stage

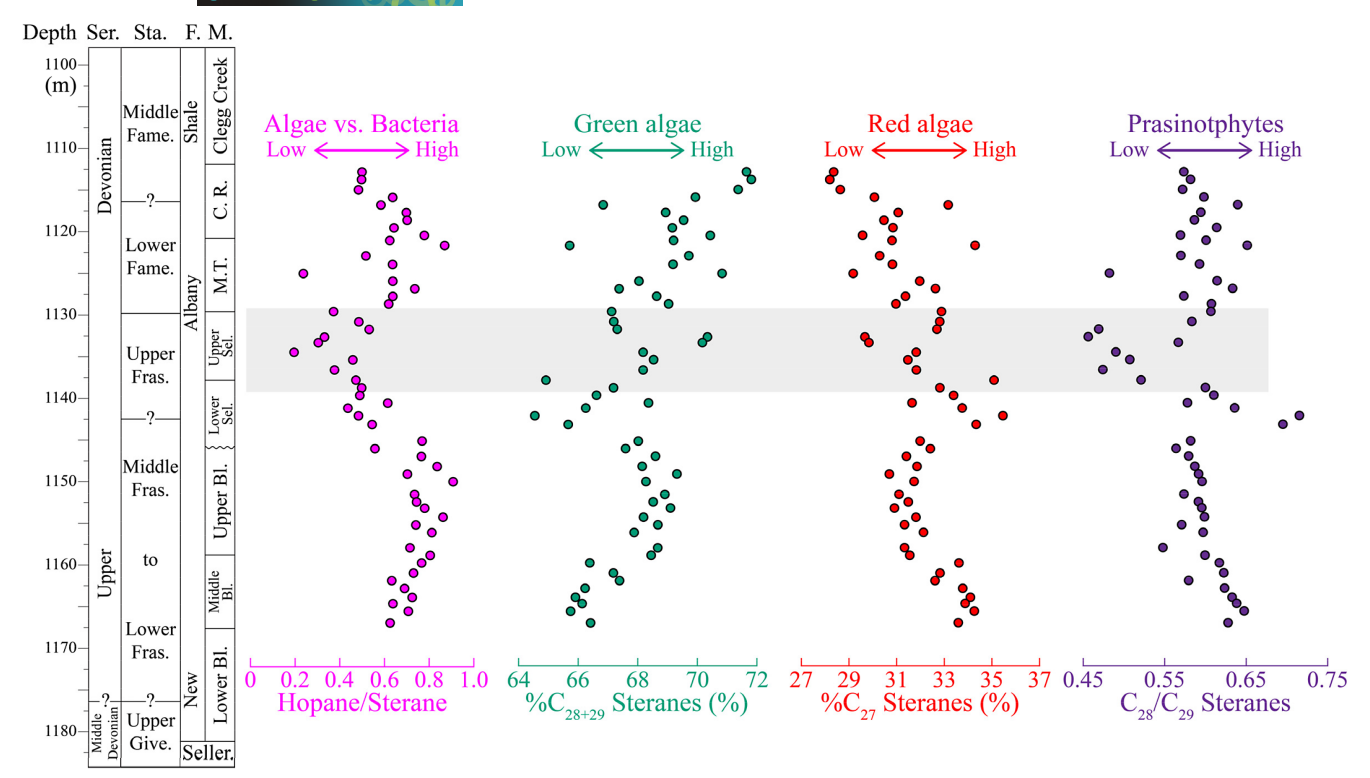


FIGURE 5 Biomarker stratigraphic profiles of the Upper Devonian New Albany Shale from the Illinois Basin (core T-6590). Hopane/ Sterane: concentration ratio of C_{27} and C_{29-35} hopanes to C_{27-29} steranes; C_{27} steranes: concentration ratio of C_{27} steranes to the sum of C_{27} , C_{28} , and C_{29} steranes; C_{28} steranes: concentration ratio of the sum of C_{28} and C_{29} steranes to the sum of C_{27} , C_{28} and C_{29} steranes: concentration ratio of C_{28} steranes. The gray area highlights the F-F mass extinction interval. Bl.—Blocher; C.R.—Camp Run; F.—Formation; Fame.—Famennian; Fras.—Frasnian; Give.—Givetian; M.—Member; M.T.—Morgan Trail; Sel.—Selmier; Seller.—Sellersburg; Ser.—Series; Sta.—Stage

(Figure S10). The hopane/sterane ratio is calculated as the concentrations of C_{27-35} hopanes divided by those of C_{27-29} steranes. The values of this ratio are lower during the F-F interval (0.37 ± 0.10) than those from the strata underlying (0.65 ± 0.11) and overlying (0.57 ± 0.13) the interval (Table 1; Figure 5). The ratios of $C_{27}/_{C27-29}$ steranes decrease and $C_{28+29}/_{C27-29}$ steranes increase during the F-F interval, but unlike other proxies, their shifts continue after the interval. The ratios of $C_{28}/_{C29}$ sterane are lower during the F-F interval (0.53 ± 0.06) than in the strata preceding (0.61 ± 0.04) and following (0.59 ± 0.04) the interval. (Table 1; Figure 5).

4.3 | Compound-specific carbon isotope

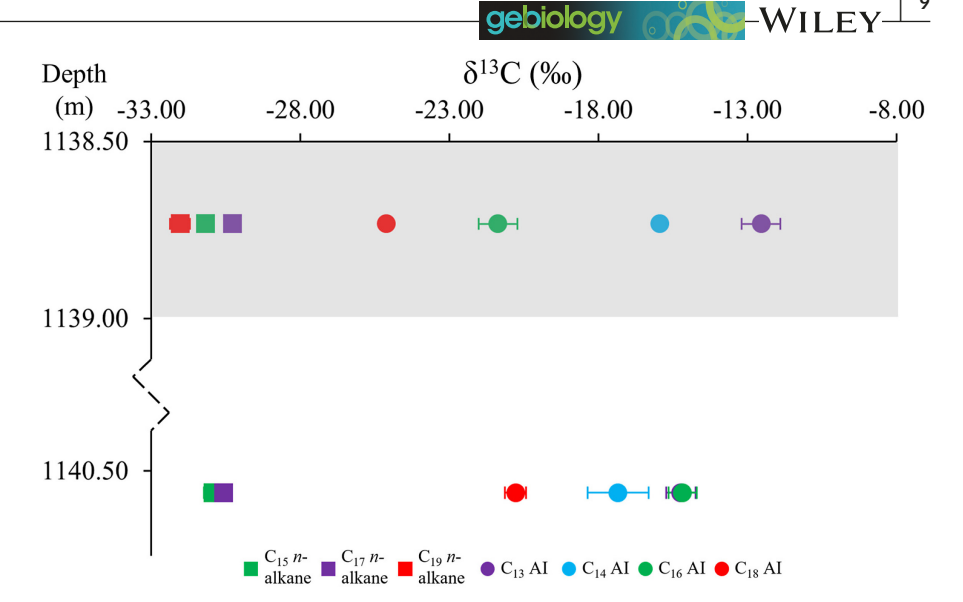
 δ^{13} C values of short-chain (C₁₃ to C₂₁) n-alkanes and aryl isoprenoids (C₁₃, C₁₄, C₁₆, and C₁₈) are measured for one sample from the mass extinction and on sample form the pre-extinction strata (Figure S11). During the mass extinction, C_{15,17,19} n-alkanes show lower δ^{13} C values (-32.0% \pm 0.3% to -30.3% \pm 0.1%) than the aryl isoprenoid δ^{13} C values (-25.1% \pm 0.2% to -12.5% \pm 0.7%; Figure 6). Similarly, for the pre-mass extinction sample, the C_{15,17,19} n-alkane δ^{13} C values (-30.9% \pm 0.3% to -30.6% \pm 0.02%) are lower than the aryl isoprenoid δ^{13} C values (-20.8% \pm 0.4% to -13.5% \pm 1.4%; Figure 6).

5 | DISCUSSION

5.1 | Environmental fluctuations across the F-F mass extinction

A series of proxies are used to infer marine redox conditions. Sedimentary aryl isoprenoids with a 2,3,6-trimethyl substitution pattern and isorenieratane (and possibly paleorenieratane that usually correlates with isorenieratane) are derived from green sulfur bacteria (Chlorobiaceae) that require both sunlight and H2S for anoxygenic photosynthesis, and hence they are commonly used as biomarkers for photic euxinia zone (PZE; Grice et al., 2005; Summons & Powell, 1986). In our samples, isorenieratane and paleorenieratane are not detected (expected when T_{max}≥438°C; Requejo et al., 1992), but the δ^{13} C values of aryl isoprenoids are more positive relative to those of algae-derived, short-chain n-alkanes (Figure 6), confirming that aryl isoprenoids were produced via the reductive tricarboxylic acid (TCA) cycle used by Chlorobium (Koopmans et al., 1996; Summons & Powell, 1987). Previous studies of the F-F strata from the Illinois Basin and neighboring Appalachian Basin detected both aryl isoprenoids and isorenieratane, supporting green sulfur bacteria as the biological source of isoprenoids (Haddad et al., 2016, 2018; Percival et al., 2022). The highly variable but overall elevated TOCnormalized aryl isoprenoid concentrations through the extinction

FIGURE 6 δ^{13} C values of C_{15,17,19} n-alkanes and C₁₃, C₁₄, C₁₆, and C₁₈ aryl isoprenoids from the mass extinction and pre-mass extinction strata. Al—2,3,6-trimethyl aryl isoprenoid. Error bars represent the standard deviation calculated from duplicate analyses of the same sample. The gray area highlights the mass extinction interval.



interval (Figure 4) indicate a more intensive photic euxinia zone (PZE) in the Illinois Basin. The frequency of PZE can be assessed by AIR, based on the premise that intermediate-chain (C₁₈₋₂₂) aryl isoprenoids are preferentially degraded to short-chain (C_{13-17}) counterparts under episodic euxinia (Schwark & Frimmel, 2004). Lower AIRs point to more stable and frequent PZE, whereas higher AIRs document more episodic occurrences. The use of AIR, however, requires the exercise of caution because of its sensitivity to weathering (Marynowski, Kurkiewicz, et al., 2011). In the study core, the mass extinction interval shows lower AIRs but elevated TOC-normalized concentrations of aryl isoprenoids (Figure 4). This pattern indicates the lower AIRs were a result of more frequent and well-established PZE, rather than a strong influence of weathering. An additional proxy used to assess the redox condition is C_{33-35} HHIs, which is based on the fact that more reducing conditions favor the preservation of C_{33} – C_{35} hopane backbone from the precursor bacteriohopanetetrol (Peters et al., 2005). C_{33-35} HHIs show a positive excursion during the F-F interval (Figure 4), which corroborates a more reducing depositional environment throughout the extinction interval.

Therefore, secular trends of biomarker redox proxies collectively demonstrate the intensification of marine euxinia in the Illinois Basin during the F-F extinction interval. Our observation is consistent with PZE biomarkers extensively detected in strata from Late Devonian epicontinental seas and basins worldwide, including Europe, North America, South America, and Africa (Lu, Lu, Ikejiri, Sun, et al., 2021), although the onset, tempo, and magnitude of PZE appear to vary spatially. For example, Percival et al. (2022) reported a concentration peak of isorenieratane below the F-F boundary in the Kowala section (Poland) and a smaller peak at the F-F boundary in a drill core from the Illinois Basin (Iowa). Lu, Lu, Ikejiri, Sun, et al. (2021) observed that the variation in PZE biomarkers from the Appalachian Basin exhibited precession-driven cyclicity during the UKW. In the present study, TOC-normalized aryl isoprenoids show considerable variations during the extinction interval, suggesting that the formation of PZE may have occurred sporadically rather than continuously, but the fluctuations in the levels of AIR and C33-35HHI are

comparatively minor. These findings support widespread development of PZE during the F-F transition, but also highlight the need for further sampling at finer temporal resolutions that are spatially comparable to determine the onset and duration/frequency of euxinia. Nonetheless, several recent studies with improved temporal resolutions or utilizing multiple proxies have increasingly recognized the intermittent nature of the Late Devonian marine anoxic events worldwide (Boyer et al., 2021; Haddad et al., 2016; Haddad et al., 2018; Lu, Lu, Ikejiri, Sun, et al., 2021; Martinez et al., 2018).

Marine euxinic zone development has been previously attributed to chemocline shoaling and oxygen minimum zone (OMZ) expansion and intensification (Schwark & Frimmel, 2004; Song et al., 2021). One commonly argued mechanism is the development of shallow water eutrophication, which would have supplied excessive organic matter for respiration and decomposition (Carmichael et al., 2019). Our n-alkane data can be used to evaluate changes in marine primary production. Short-chain n-alkanes (C_{15} , C_{17} , and C_{19}) mainly originate from algae and bacteria (Han et al., 1968), and their concentrations relative to TOC have been used as an indicator for marine primary production in geological marine settings (Lu, Lu, Ikejiri, Sun, et al., 2021). The higher TOC-normalized concentrations of nalkanes from the F-F interval (Figure 3) indicate elevated marine primary production, which could have greatly enhanced organic carbon burial and bacterial sulfate reduction to sulfide. If sulfide sequestration was restrained by iron limitation, H₂S gas would diffuse into the upper water column, leading to the formation of PZE as observed in the Illinois Basin here and other epicontinental seas during the F-F mass extinction (Haddad et al., 2016; Lu, Lu, Ikejiri, Sun, et al., 2021). However, TOC values are low during the extinction interval, which is unexpected for a productive marine system. The low TOC values can be attributed to the dilution caused by land-derived siliciclastic influxes, which will be elaborated on in the following sections.

Four indices are employed collectively to evaluate the input of terrestrial materials. TAR and CPI are alkane-based indices that can indicate shifts in organic matter sources. TAR is based on the premise that long-chain n-alkanes (C_{27} , C_{29} , and C_{31}) mainly originate from

of use; OA articles

terrestrial plant waxes (Eglinton & Hamilton, 1967), and short-chain n-alkanes (C₁₅, C₁₇, and C₁₉) are primarily derived from photosynthetic bacteria and eukaryotic algae (Han et al., 1968). A high CPI (>1) may indicate significant contributions of land plant input to marine sediments, as land-plant organic matter shows the dominance of odd-carbon-numbered alkanes in the high-carbon number range (Moldowan et al., 1985). The use of TAR and CPI requires caution as they are sensitive to thermal maturity, but vertical variations of these proxies in a limited stratigraphic range are useful to assess changes in relative contributions of land vs. aquatic flora over time (Peters et al., 2005). In our samples, neither TAR nor CPI exhibits a significant correlation with $\beta\beta/(\beta\beta+\alpha\alpha)$ C₂₉ sterane (TAR: Pearson r=0.146, p=0.288, n=55; CPI: Pearson r=0.173, p=0.208, n=55), and both indices show elevated values during the F-F interval (Figure 3), suggesting higher relative contributions of terrestrial organic matter.

Two hopane-based indices are also assessed to reflect terrestrial vs. aquatic source shifts, C₃₀ moretane/C₃₀ hopane and the diahoapen index (Figure 3). When thermal maturity is not the cause of variability, higher C_{30} moretane/ C_{30} hopane ratios can be a result of increased terrestrial plant organic matter input, elevated soil hopanoid input, and a larger clay contribution to marine sediments (French et al., 2012; Xie et al., 2007). All these three processes are associated with the input of terrigenous materials. Diahopanes are thought to originate from bacterial hopanoid precursors that have undergone oxidation and rearrangement by clay-mediated catalysis, and a higher value of the diahopane index is observed in terrigenous clay-rich rocks deposited in suboxic environments (Peters et al., 2005). Throughout the core, C_{30} moretane/ C_{30} hopane shows a significant inverse relationship with $\beta\beta/(\beta\beta+\alpha\alpha)$ C₂₉ sterane (Pearson r = -0.285, p = 0.035, n = 55), which indicates the influence of thermal maturity variation. However, the cross plot of these two parameters does not show a strong pattern (Figure S12), suggesting that higher terrestrial/soil organic matter or detrital clays could also have played a part in the elevated values during the F-F interval. The diahopane index, on the other hand, is not significantly correlated with $\beta\beta/(\beta\beta+\alpha\alpha)$ C₂₉ (Pearson r=0.215, p=0.114, n=55). Also, the higher values of this index during the extinction interval coincide with increased occurrences of grey shales (Figure 2). This pattern suggests larger quantities of siliciclastic materials from the land were introduced, leading to a greater influx of detrital clays that ultimately catalyzed the formation of diahopanes.

The four proxies, TAR, CPI, C_{30} moretane/ C_{30} hopane, and diahopane index, do not show significant, positive correlations, likely because they are all influenced by co-regulating factors other than terrigenous inputs, and the relative magnitude of terrigenous inputs versus other regulating factors can vary throughout the core. However, all proxies exhibit positive shifts of varying magnitudes during the F-F interval (Figure 3), and the common denominator that can drive these contemporaneously elevated values is greater influxes of terrigenous materials, including plant/soil organic matter and detrital clays. Other relevant factors cannot explain the simultaneous increases of the four proxies. For example, thermal maturity

will drive C_{30} moretane/ C_{30} hopane and the diahopane index in opposite directions. A more oxic dispositional environment can lead to higher values of C_{30} moretane/ C_{30} hopane and the diahopane index (French et al., 2012; Wang et al., 2018), but redox proxies discussed above indicate more reducing conditions during the F-F interval. Furthermore, the alteration in lithology observed during the extinction interval also points to a greater influx of siliciclastic materials from terrestrial sources and the resultant dilution of marine sediments. These converging lines of evidence collectively allude to a heightened terrestrial influx during the F-F interval. As all biomarker proxies also vary with factors other than terrigenous inputs, a shift of a singular proxy, such as elevated values of the diahopane index at the base of the core (Figure 3), is not sufficient to indicate changes in aquatic vs. terrigenous sources.

Our interpretation of increased terrigenous inputs during the F-F interval corroborates with existing literature that underscores the importance of land-derived nutrient runoff in bolstering marine production and creating sulfide-rich, oxygen-depleted conditions in the Late Devonian seas and basins (Kaiho et al., 2013; Lu et al., 2019; Lu, Lu, Ikejiri, Sun, et al., 2021; Tribovillard et al., 2004). The augmented terrigenous influxes could potentially be attributed to the colonization of rooted vascular plants (Algeo et al., 1995; Lu et al., 2019) and associated wildfire expansion (Lu, Lu, & Ikejiri, 2021), climatic oscillations leading to increased river runoff (Lu, Lu, Ikejiri, Sun, et al., 2021), intensified continental weathering (Percival et al., 2019), and the distance to the paleoshoreline due to eustatic oscillations (Hallam & Wignall, 1999). Our data do not directly support or refute any of these hypotheses. The magnitude of terrestrial-marine interactions appears to vary geographically during the Late Devonian (Carmichael et al., 2019), and sampling at enhanced temporal resolutions may be the key to better constraining the influence of these interactions, both at local and broader spatial scales. One example comes from a recent study of the Chattanooga Shale deposited in the adjacent Appalachian Basin. The study employed high-resolution (1-cm) sampling across the UKW interval and demonstrated temporal synchronicity between land material pulses and oceanic PZE episodes, as well as identifying cyclicities that were driven by astronomical forcing (Lu, Lu, Ikejiri, Sun, et al., 2021).

5.2 | Microbial community changes across the F-F mass extinction

5.2.1 | Relative abundance of eukaryotes vs. prokaryotes

The importance of bacterial relative to algal source organism inputs to marine sediments can be inferred by the relative abundance of hopanes vs. steranes preserved in sedimentary rocks. Hopanes are derived from bacteriohopanepolyols that are exclusively produced by bacteria, whereas steranes are primarily produced by eukaryotic sterols (Peters et al., 2005; Volkman et al., 1998). The mean hopane/sterane ratio of the study core (0.62 ± 0.16)

is at the lower end of the typical range for Phanerozoic source rock (0.5-2.0; Peters et al., 2005). The low hopane/sterane values observed here are consistent with previously reported values (≤~1) for the Frasnian to Famennian coverage in epicontinental basins and seaways (Haddad et al., 2016; Martinez et al., 2018; Marynowski, Rakocinski, et al., 2011; Song et al., 2021). By contrast, much higher values were found in a Late Ordovician epeiric sea setting, where the average baseline was ~4.0-6.0 and excursions were up to ~12 (Rohrssen et al., 2013). Even higher values were reported for the Meishan section in South China, showing excursions to 31-70 before and after the Permian-Triassic boundary (Cao et al., 2009). The low hopane/sterane ratios that have been reported for the Late Devonian marine basins indicate the dominance of eukaryotic algae as primary producers, which is a typical character of a productive marine ecosystem. Sediments in marine settings with high productivity tend to have lower hopane/ sterane ratios than those from contemporaneous oligotrophic settings (Haddad et al., 2016; Martinez et al., 2018). The same trend has been also noted for modern oceans—the ratio of eukaryotic to bacterial biomass is usually lower in oligotrophic settings than in mesotrophic to eutrophic settings (Pehr et al., 2018). Bacteria biomass can dominate the microbial biomass in oligotrophic ocean sites, yet algae are usually the dominant primary producer in nutrient-rich coastal oceans (Fuhrman et al., 1989).

The hopane/sterane ratios (calculated as C₂₇₋₃₅ hopanes/C₂₇₋₂₉ steranes) display an evident decrease during the F-F transition (Figure 5), suggesting a more prominent eukaryotic dominance in the microbial community during the extinction interval. This observation reinforces the interpretation of increases in shallowwater productivity during the F-F mass extinction. Terrigenous nutrient influx stimulated algal primary productivity, inducing a high-abundance but likely low-diversity algal ecosystem. This scenario is similar to what is observed in modern coastal oceans experiencing cultural eutrophication (Diaz et al., 2004; Diaz & Rosenberg, 2008; Malone & Newton, 2020). Previous works have also reported changes in bacterial vs. algal abundance during various biocrises, and variable environmental triggers have been postulated, including temperature, nutrient availability, and OMZ extent. For example, bacterial primary production in the Late Ordovician tropical seas was linked to a warm climate and resultant OMZ expansion, whereas eukaryotic production was higher when the ocean was cooler with contracted OMZs (Rohrssen et al., 2013; Smolarek et al., 2017). Similarly, heightened bacteria primary productivity was tied to intervals with enhanced water column stratification and oxygen depletion, based on biomarkers from the Permian-Triassic succession in Meishan, South China (Cao et al., 2009). In their study, the proliferation of bacterial biomass in the Early Triassic was interpreted as a result of the persistence of conditions unfavorable for O₂-respiring organisms in the marine photic zone prior to the Permian-Triassic extinction. Notably, these observations contrast our findings showing a more pronounced dominance of eukaryotic production during the F-F interval with expanded OMZs. This difference may be related to the extent and duration of oxygen depletion/stress, as well as other relevant environmental factors (e.g., nutrient availability) that can alter the relative abundance of algal and bacterial biomass.

5.2.2 | Algal community composition

Sterane carbon number distribution can reflect changes in algal communities through time and provide insights into algal diversification and evolution (Schwark & Empt, 2006). In Paleozoic rocks, C28 and C₂₀ steranes are used to indicate the presence of green algae, and C₂₇ steranes are diagnostic biomarkers for red algae (Rhodophyta; Schwark & Empt, 2006). Thus, we use $%C_{27}$ and $%C_{28+29}$ steranes to track changes in the relative abundance of red and green algae, respectively. Throughout the study core, the percentage contributions of C₂₈₊₂₉ exceed 50% (Figure 5), indicating the dominance of green algae. This finding is consistent with prior studies conducted on other Late Devonian sections (Haddad et al., 2016; Martinez et al., 2018; Song et al., 2021) and supports the known evolution pattern of algae (Schwark & Empt, 2006). During the F-F interval, $%C_{27}$ sterane became lower and $%C_{28+29}$ sterane became higher, which indicates green algae became more dominant over red algae. Green algal clades compete well in oligotrophic settings due to their small cell size and competence to grow on various nitrogen species (Parker et al., 2008). In contrast, red algae preferentially flourish in mesotrophic-eutrophic conditions irrespective of temperature and light penetration, as observed in modern and paleo-oceans (Halfar & Mutti, 2005). In this study, red algae did not increase during the F-F interval, despite our interpretation of increased terrigenous nutrient influx. This may indicate that nutrients were not adequately abundant to favor red algae, or that nutrient availability was not the dominant factor modulating green vs. red algal abundances in the Late Devonian Illinois Basin. Furthermore, unlike other microbialcommunity biomarker parameters, the decreasing trend of $%C_{27}$ sterane and increasing trend of C_{28+29} sterane continued after the extinction interval. These lasting changes may indicate that algal community compositions were more responsive to a long-term environmental driver, such as water salinity, as green algae have a greater salinity tolerance (Song et al., 2021). Using B/Ga as a paleo-salinity indicator, Song et al. (2021) found that a reduction in water-mass salinity coincided with a shift to greater dominance of green algae in the Late Devonian marine seaway from Frasnian to Famennian. However, we were unable to test this hypothesis here as boron data were not collected.

The C_{28}/C_{29} sterane ratio can reflect changes in green algal assemblage, providing information on the relative abundance of C_{28} sterol-producing algae vs. more primitive C29 sterol-producing algae (Schwark & Empt, 2006). Prasinotphytes (Chlorophyta) are thought to be the primary taxon of green algae producing C_{28} -dominating sterol (Kodner et al., 2008; Schwark & Empt, 2006; Volkman et al., 1994), and thus, C_{28}/C_{29} sterane ratios in geological records have been linked to the relative abundance of prasinophytes within green algae (Kodner et al., 2008; Schwark & Empt, 2006). The

.4724669, 0, Downloaded from https://onlinelibrary.wiley.com/doi/10.1111/gbi.12568 by Auburn University Libraries

Wiley Online Library on [05/08/2023]. See the Terms and Conditions (https://or

and-conditions) on Wiley Online Library for rules of use; OA articles

are governed by the applicable Creative Commons

decrease during the F-F interval (Figure 5) can be interpreted as a recession of prasinophytes, assuming this ratio mainly reflects green algal sources. However, this interpretation contrasts with our expectation since prasinophyte algae, the resilient "disaster taxa" green algae, compete particularly well under oxygen-depleted conditions and usually prosper during mass extinction events (Tappan, 1980). Furthermore, organic-walled microfossils, to which prasinophytes are considered to be an important contributor, showed a large increase and remained high during the F-F mass extinction interval in the Walnut Creek section, Appalachian Basin (western New York; Kelly et al., 2019). Since the prior evidence, although limited, mostly pointed to increases in prasinophyte across the F-F transition, the lower C₂₈/C₂₉ sterane ratios observed here likely reflect other modulating factors. The C_{28}/C_{29} sterane ratio can be influenced by the input of terrestrial plants that also produce significant quantities of C_{29} sterols (Peters et al., 2005). One possibility is the higher influxes of terrigenous materials that the Illinois Basin likely experienced during the F-F interval (Figure 3). This shift could have contributed to the observed decline of the C_{28}/C_{29} sterane ratio, potentially overprinting the changes associated with variations in green algal community composition. Additional data, such as the stable carbon isotopic compositions of steranes, will be needed to assess the significance of terrestrial sources in influencing this ratio.

5.2.3 | Bacteria producing 2-methylhopanoids and the N Cycle

The 2α -MHI was initially used as a proxy to reconstruct cyanobacterial activities in ancient marine environments, including intervals associated with mass extinction events (Sepulveda et al., 2009; Xie et al., 2005, 2007). However, more recent cultural and genomicbased evidence indicates 2-methylhopanoids, the precursor of 2α -methylhopanes preserved in geological records, have more diverse biological sources beyond N-fixing cyanobacteria (Naafs et al., 2022; Welander et al., 2010). A review of the geological record reveals that 2α-methylhopanes increased significantly (exceeding 15%) during certain events marked by significant climatic and biotic shifts in the Phanerozoic era. As such, the 2α -MHI index is now recognized as an indicator of bacteria experiencing stress and/or a shift of a specific ecological niche characterized by poor oxygen and limited fixed nitrogen (Naafs et al., 2022). The 2α -MHIs $(0\%-3.12\%, 1.84\%\pm0.74\%)$ in the study section are comparable to some reported from the Late Devonian strata, i.e., ~1%-8% for the Frasnian through Famennian coverage in the Appalachian and Madre de Dios Basins (Haddad et al., 2016), 1.5%-5.9% for the Grass Creek Shale from the Illinois Basin (Percival et al., 2022), and <5% for the end-Devonian Cleveland Shale in the Appalachian Basin (<5%; Martinez et al., 2018). These values, however, are overall lower than those reported from the Famennian sequence (6.1%-13.4%; Marynowski, Rakocinski, et al., 2011) and the Frasnian-Famennian sequence (up to 17.3%) of the Kowala Quarry section, Poland (Percival et al., 2022).

In the study core, the 2α -MHIs (1.43% \pm 1.27%) during the F-F interval are more variable and have a slightly lower mean value compared to the pre- and post-F-F strata, mostly due to the occurrence of several samples with undetected 2α -methylhopanes (Figure 4). A likely contributing factor is the increased frequency of grey shale, which has reduced levels of TOC and hence made it more challenging to detect low-concentration biomarkers. A significant positive correlation between TOC and 2-MHI during the extinction interval (Pearson r=0.27, p=0.046) supports this speculation. When intervals with undetected 2α -methylhopanes are removed from the analysis, a slight increase in 2α -MHI (2.38% \pm 0.42%) is observed during the F-F interval relative to those before (2.07% ±0.37%) and after $(1.73\% \pm 0.69\%)$ the interval. However, the magnitude of this shift (<1%) is small, particularly in comparison to those reported for several major events. For example, shifts up to ~50% have been documented in the Permian-Triassic boundary section at Meishan in South China (Cao et al., 2009; Xie et al., 2007), while shifts up to about 30% have been reported for a Cretaceous-Paleogene boundary layer in Denmark (Sepulveda et al., 2009) and in shales deposited throughout Europe during the Toarcian oceanic anoxic event (OAE; Farrimond et al., 2004). As such, the shift in 2α -MHI during the F-F interval does not seem to be significant enough to suggest that major perturbations took place in marine biogeochemistry and environmental niches that led to significant stress to bacteria in the Illinois Basin. Our study is not the first noting the lack of large changes in 2α -MHIs associated with the F-F transition. Haddad et al. (2016) did not observe evident increases in 2α -methylhopane concentrations within the F-F strata located in both the Appalachian Basin and Madre De Dios Basin. Percival et al. (2022) analyzed 2α -MHIs from the F-F strata deposited in the Illinois Basin (Iowa) and Checiny-Zbrza Basin (Kowala Quarry, Poland). Although they highlighted positive shifts in the index below the F-F boundary, the shift from the Illinois Basin is small (<5%), which is consistent with our finding. The Checiny-Zbrza Basin exhibited the only relatively large shift (>10%) reported for the F-F transition to date; however, this shift is still relatively small compared to many shifts (>15%) associated with other major events marked by significant climatic and biotic changes throughout the Phanerozoic era (Naafs et al., 2022).

The discussion of 2α -MHI is frequently linked to changes in sedimentary $\delta^{15}N$ values because both proxies are relevant indicators of N-cycling processes (Haddad et al., 2016; Percival et al., 2022). Bulk sedimentary $\delta^{15}N$ values usually reflect $\delta^{15}N$ of marine dissolved inorganic nitrogen (DIN). In a general sense, $\delta^{15}N$ values (0%–3%) in the study core fall in the range expected for nitrate as the dominant reactive species and planktonic biomass being dominated by eukaryotic communities (Whalen et al., 2015), which agrees with the low H/S ratios observed in the present study. Shifts in $\delta^{15}N$ during the Late Devonian strata have been largely interpreted as the relative dominance of nitrogen fixation vs. denitrification in the marine N cycle (Whalen et al., 2015). These shifts often reflect N perturbations, which appears to depend on local factors and processes because shifts of variable magnitudes, directions, and durations have been documented throughout the F-F transition (Carmichael

and-conditions) on Wiley Online Library for rules of use; OA articles are governed by the applicable Creative Commons

et al., 2019). For example, negative excursions were observed in the Illinois Basin (Iowa) and Chęciny–Zbrza Basin (Poland) across the F-F boundary, which have been attributed to either increased nitrogen fixation or reduced denitrification (Percival et al., 2022). Positive excursions were observed at the onset of the UKW event from the basins of Western Canada and South China, and they were thought to be a result of the increasing importance of denitrification in the N cycle (Whalen et al., 2015). No evident changes were observed for the F-F strata from the Appalachian and Madre De Dios Basins (Haddad et al., 2016) as well as from the Namur-Dinant Basin, Belgium (Percival et al., 2022), which could be a result of lack of major N perturbations or several mechanisms operating and obscuring each other's effect.

In the study core of the New Albany Shale, the F-F interval shows overall higher $\delta^{15}N$ values compared to other sections of the core (Figure 2). The first plausible explanation is the expansion of the denitrification zone owing to elevated primary production. Water column denitrification results in isotopic fractionation (ε) of ~+20% and sedimentary denitrification has ε of 0%. During the F-F interval, increases in shallow-water algal productivity (evidenced by elevated short-chain alkanes concentrations and larger H/S ratios) could have led to oxygen depletion at the lower water column. This may have allowed denitrification, which was originally confined to sediments, to expand into the water column. Because $\delta^{15}N$ values remained relatively high in the F-F interval, we infer that despite the intensified PZE and expanded OMZ, the level of oxygen starvation had not reached a point where N-fixation ($\varepsilon = -1\%$) was favored to lower δ^{15} N values. This interpretation aligns with the lack of significant shifts in 2-MeHI during the F-F interval (Figure 4).

Another consideration is lithological changes and their association with terrigenous N input. The F-F interval is characterized by an increased frequency of grey shales interbedded with black shales (Figure 2). A previous study has noted that δ^{15} N of grey shales are more positive than $\delta^{15}N$ of interbedded black shales deposited during the Late Devonian (Uveges et al., 2019). The reason behind the elevated $\delta^{15}N$ values in grey shales remains speculative. One interpretation is that grey shales were deposited in cooler environments, which allowed better basinal oxygenation and favored the dominance of nitrate and denitrification (Uveges et al., 2019). UKW coincides with short, abrupt cooling episodes globally (Chen et al., 2021; Huang et al., 2018; Joachimski et al., 2009; Joachimski & Buggisch, 2002), but our data do not provide evidence suggestive of a more oxygenated environment in the Illinois Basin during the F-F interval. Another plausible interpretation is that organic-lean grey shales are more susceptible to the influence of clay-attached N. The TN vs TOC plot shows a strong, positive correlation between the two parameters. The linear fitting liner has an intercept of $\sim 0.17\%$ (TN (%)=0.0271*TOC (%)+0.1731, R^2 =0.93), which can be interpreted as the amount of inorganic N associated with clay minerals. This contribution accounts for an estimated 87% of the total N within the extinction interval and around 47% of the total N outside the interval. The inorganic N can be derived from marine organic N remineralization or terrigenous sources. The former process

produces ¹⁵N-depleted ammonium but meanwhile leads to ¹⁵N enrichment in sedimentary organic matter, thus producing little net change in bulk sedimentary $\delta^{15}N$ (Uveges et al., 2019). On the other hand, terrigenous inorganic N entering coastal oceans can vary in a large range (Montoya, 2008). In order to account for the observed increase (<+1%) in δ^{15} N during the F-F interval, δ^{15} N of terrigenous inorganic N needs to be ~ +2.5% more positive than that of marine inorganic N, assuming all clay-attached inorganic N is terrigenous. This magnitude of difference is plausible based on data from modern systems, e.g., median $\delta^{15}N$ is ~7 % for modern river nitrate and $\delta^{15}N$ for modern ocean nitrate is ~5% (Matiatos et al., 2021; Sigman & Casciotti, 2009). This interpretation also aligns with our data of TAR, CPI, C₃₀ moterane/hopane, and diahopane index, which point to higher input of terrigenous materials during the F-F interval. Furthermore, this hypothesis agrees with a widely-cited idea that the early forestation of the Late Devonian can lead to transient intensification of pedogenesis, forming productive soils that exported N nutrients to oceans (Algeo et al., 1995).

5.2.4 | Methanotrophs

Type I methanotrophs and some acetic acid bacteria are identified as primary source organisms for 3β-methylbacteriohopanepolyols that are biological precursors of 3β-methylhopanes in sedimentary records (Zundel & Rohmer, 1985). The ratio of 3β-methylhopanes relative to their non-methylated hopane counterpart (i.e., 3β-MHI) has been used to depict the abundance of methanotrophs in ancient oceans (Farrimond et al., 2004; Summons et al., 1999). The 3-methylhopane index values found here(0%-4.02%; Figure 5) are moderate in value, and typical of Late Devonian sedimentary rocks from marine shelf environments (Haddad et al., 2016; Martinez et al., 2018) getting up to 4%, but these are much lower in magnitude in comparison with Ordovician (Rohrssen et al., 2013) and Silurian (Marshall et al., 2023) marine rocks which often yield values in the 5%-15% range. Furthermore, these values are lower than those reported for end-Triassic strata in the UK (0%-16%; Fox et al., 2020) and Canada (0%-5%; Kasprak et al., 2015) and Permian-Triassic strata in South China (0%-10%; Cao et al., 2009). Although the 3-methylhopane index values throughout the study core are not particularly high, the values during the extinction interval surpass those of the strata above and below (Figure 4), indicating an increased presence of methanotroph biomass and implying a heightened methane cycling process. Methanotrophic bacteria are microaerophilic and most active in the aerobic-anaerobic transition zone (Farrimond et al., 2004). Therefore, our observation can be explained by intensified oxygen scarcity during the F-F event, which stimulated strictly anaerobic methanogens and increased CH₄ supplies to methanotrophic bacteria. Our results add to prior evidence that methanotrophs exhibit sensitivity to dramatic environmental and climatic perturbations. Rohrssen et al. (2013) linked reductions in methanogenesis and methanotrophy to cooling-driven O2 increases and associated OMZ contraction in Late Ordovician tropical

14724669, 0, Downloaded from https://onlinelibrary.wiley.com/doi/10.1111/gbi.12568 by Auburn University Libraries, Wiley Online Library on [05/08/2023]. See the Terms and Conditions (https://onlinelibrary.wiley.

on Wiley Online Library for rules of use; OA articles are governed by the applicable Creative Commons

seas. Cao et al. (2009) related the exceptionally high 3β-MHI values (1.6%-7%) of the Meishan Permian-Triassic section to heightened methane oxidation coupled to active methanogenesis in an oxygen- and sulfate-depleted environment. Our data offer further confirmation of the susceptibility of the methanotroph population to fluctuations in marine redox conditions.

5.3 | Marine microbial community structure responses to mass extinction events: Implications for changes in modern coastal oceans

Our biomarker data provide new evidence for community-level changes in marine microbes under the impact of environmental and biogeochemical disturbances during the F-F mass extinction event. We note that the observed changes are relatively transient and limited to the duration of the mass extinction interval, as shown by that the analyzed microbial biomarker parameters (with the exception of green vs. red algal abundance) returned to the pre-disturbance level immediately following the extinction. These observations may suggest either that the Illinois Basin provided an isolated environment that did not mirror the severity of environmental degradation that occurred at a broad spatial scale, or that the Late Devonian marine microbial community was overall resilient to substantial, short-term disturbances in oxygen and nutrient availability. The latter interpretation appears to be more likely, as previous studies also noted the overall lack of large, abnormal changes in methylhopane parameters (Boyer et al., 2021;

Haddad et al., 2016; Percival et al., 2019). More lasting changes involving the emergency of new community structures probably require environmental disturbances at a greater magnitude. Certainly, this interpretation needs to be taken with the caveat that fossil biomarkers are related to specific biosynthetic pathways and do not offer ecological response information at a detailed taxonomic level.

A number of cases have been studied in detail to understand community-level microbial changes during biocrises. Nevertheless, the Late Devonian changes we observed here warrant further discussion in that they show some key features that are different from those observed for some other mass extinction events, e.g., the Permian-Triassic mass extinction event (Cao et al., 2009; Xie et al., 2017). Speculating on the causality of such differences provides clues regarding how mass extinction events can ecologically restructure marine microbial communities. For the Late Devonian mass extinction expressed in shallow marine basins, we found that the eukaryotic primary producers not only adapted but did exceptionally well. This is different from the Permian-Triassic extinction, where bacteria became more abundant over eukaryotic algae (Cao et al., 2009; Xie et al., 2017). In addition, abnormal increases in the 2α -MHI index detected in the Permian-Triassic extinction strata signify significant stress to bacteria or restructure of ecological niches (Cao et al., 2009; Xie et al., 2017), and such changes are lacking in Late Devonian seas (Haddad et al., 2016; Martinez et al., 2018; and data from this study). The F-F mass extinction identified here in the New Albany shale displays a scenario with heightened eukaryotic production

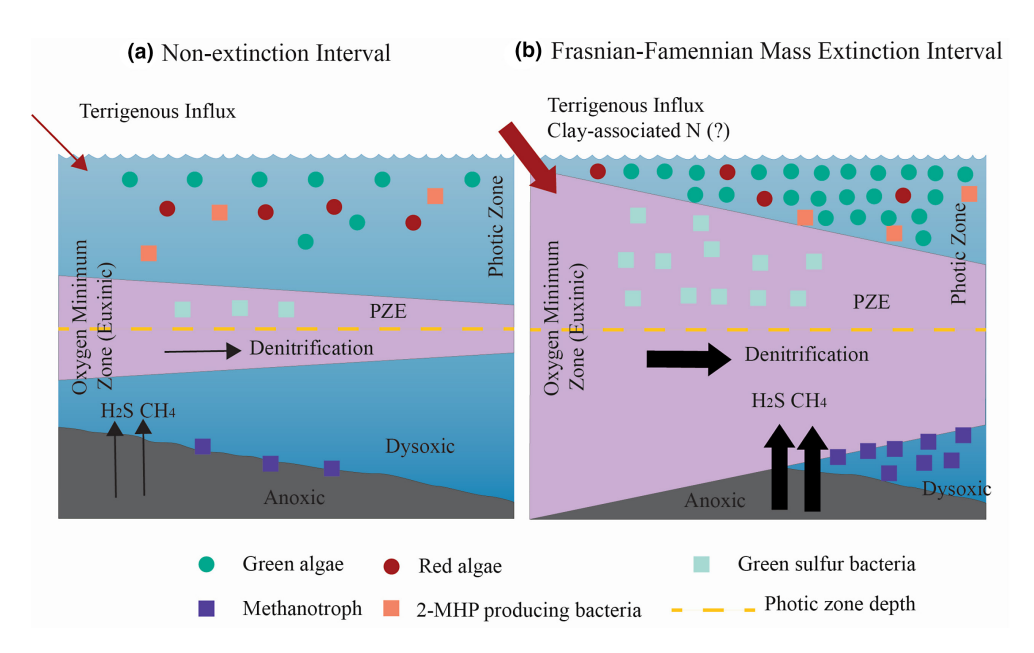


FIGURE 7 Conceptual diagram illustrating major differences in the marine microbial community between non-extinction strata and the Frasnian-Famennian mass extinction interval. Relative to Panel (a), Panel (b) shows that during the F-F event, marine algal productivity increased, featured by the proliferation of green algae. This was likely caused by increased influxes of terrigenous nutrients. As a result, the oxygen minimum zone (OMZ) expanded, which enhanced the importance of water column denitrification in the N cycle. The more reducing condition also facilitated the release of H_2S to the water column, creating photic zone euxinia (PZE) and the associated expansion of green sulfur bacteria. Methanotrophs increased due to enhanced methane fluxes under more reducing conditions, while 2-MHP-producing bacteria did not show significant changes.

gebiology WILEY 15

that appears to be influenced by terrestrial runoff (Figure 7). In such a system, energy flow through the food web was driven more by autotrophic, eukaryotic production than by heterotrophic prokaryotes via the microbial loop. This is strikingly similar to what modern coastal oceans are experiencing—excessive anthropogenic nutrients boost algal productivity in the surface ocean, leading to oxygen depletion and the demise of oxygen-sensitive organisms in the lower water column (Diaz et al., 2004; Malone & Newton, 2020). By comparison, the Permian-Triassic event recorded in the Meishan section is expressed as a 'bacterial bloom' scenario with more substantial changes in the microbial community and enhanced N-fixation. The environmental conditions became more favorable to prokaryotes, and eukaryotic production was suppressed (Cao et al., 2009; Xie et al., 2017). The food-web energy flow was switched to a mode driven more by prokaryotic producers and decomposers. Prokaryotes have been the primary regulator of the global biogeochemical cycle since the beginning of life until the evolution of energetically superior eukaryotes that now dominate Earth's major biomes (Zubkov, 2014). Bacteria can acclimate to a wider range of marine habitats than eukaryotes. The community-level turnover from eukaryotes to prokaryotes recorded in the Permian-Triassic Meishan section thus could be interpreted as a degradation to a more ancestral ecosystem. These comparisons highlight different responses at the base of food webs across major faunal mass extinction events. Future studies should strive to understand whether these differences can be linked to specific environmental stressors or propagated to organisms at higher trophic levels, to better understand the significance of microbial community shift in ecological resilience during major biotic crises.

ACKNOWLEDGMENTS

Jian Chen was supported by a Ph.D. fellowship from the China Scholarship Council and the Graduate Council Fellowship from the University of Alabama. Acknowledgments are made to the Gulf Coast Association of Geological Societies Student Grant (2019), the Geological Society of America Graduate Student Grant (2019), and the American Association of Petroleum Geologists Foundation Graduate Student Grant (2019, 2021) (to Jian Chen). The authors thank Joe Lambert, ChangFeng Zhu, LiShu Kong, KeLiang Zhou, Tian Xia, and Marieh Arekhi for assisting with geochemical analyses. Ryan Pinkston and Ray Daniel at Kentucky Geological Survey are thanked for their assistance with core access and sampling. The lithological description benefits from comments by Dr. Charles Savrda of Auburn University. Dr. Jed Day at Illinois State University is thanked for his assistance with the conodont analysis. We acknowledge Dr. Prabhakar Clement of the University of Alabama for GC-QQQ-MS facility access made possible by Alabama Water Institute and the water workforce development initiatives of the NSF grant OIA-2019561. The biomarker analyses were performed on a GC-MS purchased through support from the Instrumentation and Facilities Programs in the Division of Earth Sciences (NSF EAR-1255724 to YueHan Lu). Acknowledgments are made to the

Donors of the American Chemical Society Petroleum Research Fund (PRF#61366-ND2 to YueHan Lu).

CONFLICT OF INTEREST STATEMENT

The authors have no competing interests to declare.

DATA AVAILABILITY STATEMENT

The data that support the findings of this study are available on Dryad DOI:10.5061/dryad.dz08kps34.

ORCID

Jian Chen https://orcid.org/0000-0002-7363-2370 YueHan Lu https://orcid.org/0000-0002-0536-532X

REFERENCES

- Algeo, T. J., Berner, R. A., Maynard, J. B., & Scheckler, S. E. (1995). Late Devonian oceanic anoxic events and biotic crises: "Rooted" in the evolution of vascular land plants. GSA Today, 5(3), 64–66.
- Algeo, T. J., & Tribovillard, N. (2009). Environmental analysis of paleoceanographic systems based on molybdenum-uranium covariation. Chemical Geology, 268(3-4), 211-225.
- Azam, F., & Malfatti, F. (2007). Microbial structuring of marine ecosystems. *Nature Reviews Microbiology*, *5*, 782–791.
- Bond, D. P. G., & Wignall, P. B. (2008). The role of sea-level change and marine anoxia in the Frasnian-Famennian (Late Devonian) mass extinction. *Palaeogeography Palaeoclimatology Palaeoecology*, 263(3– 4), 107–118.
- Boyer, D. L., Martinez, A. M., Evans, S. D., Cohen, P. A., Haddad, E. E., Pippenger, K. H., Love, G. D., & Droser, M. L. (2021). Living on the edge: The impact of protracted oxygen stress on life in the Late Devonian. *Palaeogeography, Palaeoclimatology, Palaeoecology*, 566, 1-16.
- Cao, C. Q., Love, G. D., Hays, L. E., Wang, W., Shen, S. Z., & Summons, R. E. (2009). Biogeochemical evidence for euxinic oceans and ecological disturbance presaging the end-Permian mass extinction event. *Earth and Planetary Science Letters*, 281(3–4), 188–201.
- Carmichael, S. K., Waters, J. A., Konigshof, P., Suttner, T. J., & Kido, E. (2019). Paleogeography and paleoenvironments of the Late Devonian Kellwasser event: A review of its sedimentological and geochemical expression. *Global and Planetary Change*, 183, 1-17.
- Chen, B., Ma, X., Mills, B. J. W., Qie, W., Joachimski, M. M., Shen, S., Wang, C., Xu, H., & Wang, X. (2021). Devonian paleoclimate and its drivers: A reassessment based on a new conodont δ^{18} O record from South China. *Earth-Science Reviews*, 222, 1–12.
- Chen, D., Wang, J., Racki, G., Li, H., Wang, C., Ma, X., & Whalen, M. T. (2013). Large Sulphur isotopic perturbations and oceanic changes during the Frasnian-Famennian transition of the Late Devonian. *Journal of the Geological Society*, 170(3), 465–476.
- Day, J., & Witzke, B. J. (2017). Upper Devonian biostratigraphy, event stratigraphy, and late Frasnian Kellwasser extinction bioevents in the Iowa Basin: Western Euramerica. In M. Montenari (Ed.), Advances in sequence stratigraphy (Vol. 2 pp. 243–332). Elsevier.
- Diaz, R., & Rosenberg, R. (2008). Spreading dead zones and consequences for marine ecosystems. Science, 321(5891), 926–929.
- Diaz, R. J., Nestlerode, J., & Diaz, M. L. (2004). A global perspective on the effects of eutrophication and hypoxia on aquatic biota and water quality. In G. Rupp & M. D. White (Eds.), Fish physiology, toxicology and water quality (pp. 1–33). U. S. Environmental Protection Agency, Ecosystems Research Division.
- Eglinton, G., & Hamilton, R. J. (1967). Leaf Epicuticular waxes: The waxy outer surfaces of most plants display a wide diversity of

- fine structure and chemical constituents. *Science*, 156(3780), 1322-1335.
- Farrimond, P., Talbot, H. M., Watson, D. F., Schulz, L. K., & Wilhelms, A. (2004). Methylhopanoids: Molecular indicators of ancient bacteria and a petroleum correlation tool. *Geochimica et Cosmochimica Acta*, 68(19), 3873–3882.
- Fox, C. P., Cui, X., Whiteside, J. H., Olsen, P. E., Summons, R. E., & Grice, K. (2020). Molecular and isotopic evidence reveals the end-Triassic carbon isotope excursion is not from massive exogenous light carbon. Proceedings of the National Academy of Sciences of the United States of America. 117(48), 30171–30178.
- French, K. L., Tosca, N. J., Cao, C. Q., & Summons, R. E. (2012). Diagenetic and detrital origin of moretane anomalies through the Permian–Triassic boundary. *Geochimica et Cosmochimica Acta*, 84, 104–125.
- Fuhrman, J. A., Sleeter, T. D., Carlson, C. A., & Proctor, L. M. (1989).
 Dominance of bacterial biomass in the Sargasso Sea and its ecological implications. *Marine Ecology Progress Series*, 57(3), 207-217.
- Golonka, J. (2020). Late Devonian paleogeography in the framework of global plate tectonics. *Global and Planetary Change*, 186, 103129. https://doi.org/10.1016/j.gloplacha.2020.103129
- Grice, K., Cao, C. Q., Love, G. D., Bottcher, M. E., Twitchett, R. J., Grosjean, E., Summons, R. E., Turgeon, S. C., Dunning, W., & Jin, Y. G. (2005). Photic zone euxinia during the Permian-Triassic superanoxic event. *Science*, 307(5710), 706–709.
- Haddad, E. E., Boyer, D. L., Droser, M. L., Lee, B. K., Lyons, T. W., & Love, G. D. (2018). Ichnofabrics and chemostratigraphy argue against persistent anoxia during the upper Kellwasser event in New York state. *Palaeogeography*, *Palaeoclimatology*, *Palaeoecology*, 490, 178–190.
- Haddad, E. E., Tuite, M. L., Martinez, A. M., Williford, K., Boyer, D. L., Droser, M. L., & Love, G. D. (2016). Lipid biomarker stratigraphic records through the Late Devonian Frasnian/Famennian boundary: Comparison of high-and low-latitude epicontinental marine settings. Organic Geochemistry, 98, 38–53.
- Halfar, J., & Mutti, M. (2005). Global dominance of coralline red-algal facies: A response to Miocene oceanographic events. *Geology*, 33(6), 481–484.
- Hallam, A., & Wignall, P. B. (1999). Mass extinctions and sea-level changes. Earth-Science Reviews, 48(4), 217–250. https://doi. org/10.1016/S0012-8252(99)00055-0
- Han, J., McCarthy, E. D., Hoeven, W. V., Calvin, M., & Bradley, W. H. (1968). Organic geochemical studies, II. A preliminary report on the distribution of aliphatic hydrocarbons in algae, in bacteria, and in a recent lake sediment. Proceedings of the National Academy of Sciences of the United States of America, 59(1), 29–33.
- Hillbun, K., Playton, T. E., Tohver, E., Ratcliffe, K., Trinajstic, K., Roelofs, B., Caulfield-Kerney, S., Wray, D., Haines, P., Hocking, R., Katz, D., Montgomery, P., & Ward, P. (2015). Upper Kellwasser carbon isotope excursion pre-dates the F-F boundary in the upper Devonian Lennard shelf carbonate system, Canning Basin, Western Australia. Palaeogeography, Palaeoclimatology, Palaeoecology, 435, 180-190.
- House, M. R. (2002). Strength, timing, setting and cause of mid-Palaeozoic extinctions. *Palaeogeography, Palaeoclimatology, Palaeoecology*, 181(1–3), 5–25.
- Huang, C., Joachimski, M. M., & Gong, Y. (2018). Did climate changes trigger the Late Devonian Kellwasser crisis? Evidence from a high-resolution conodont $\delta^{18}{\rm O}_{\rm PO4}$ record from South China. Earth and Planetary Science Letters, 495, 174–184.
- Jiang, A. Z., Zhou, P. Y., Sun, Y. G., & Xie, L. J. (2013). Rapid column chromatography separation of alkylnaphthalenes from aromatic components in sedimentary organic matter for compound specific stable isotope analysis. Organic Geochemistry, 60, 1–8.
- Joachimski, M. M., Breisig, S., Buggisch, W., Talent, J. A., Mawson, R., Gereke, M., Morrow, J. R., Day, J., & Weddige, K. (2009). Devonian

- climate and reef evolution: Insights from oxygen isotopes in apatite. Earth and Planetary Science Letters, 284(3–4), 599–609.
- Joachimski, M. M., & Buggisch, W. (2002). Conodont apatite δ^{18} O signatures indicate climatic cooling as a trigger of the Late Devonian mass extinction. *Geology*, 30(8), 711-714.
- Kabanov, P., Hauck, T. E., Gouwy, S. A., Grasby, S. E., & van der Boon, A. (2023). Oceanic anoxic events, photic-zone euxinia, and controversy of sea-level fluctuations during the middle-Late Devonian. *Earth-Science Reviews*, 241, 1–34.
- Kaiho, K., Yatsu, S., Oba, M., Gorjan, P., Casier, J. G., & Ikeda, M. (2013).
 A forest fire and soil erosion event during the Late Devonian mass extinction. *Palaeogeography Palaeoclimatology Palaeoecology*, 392, 272–280. https://doi.org/10.1016/j.palaeo.2013.09.008
- Kasprak, A. H., Sepulveda, J., Price-Waldman, R., Williford, K. H., Schoepfer, S. D., Haggart, J. W., Ward, P. D., Summons, R. E., & Whiteside, J. H. (2015). Episodic photic zone euxinia in the northeastern Panthalassic Ocean during the end-Triassic extinction. *Geology*, 43(4), 307–310.
- Kelly, A. A., Cohen, P. A., & Boyer, D. L. (2019). Tiny keys to unlocking the Kellwasser events: Detailed characterization of organic walled microfossils associated with extinction in Western New York state. PALAIOS, 34(2), 96–104.
- Kodner, R. B., Pearson, A., Summons, R. E., & Knoll, A. H. (2008). Sterols in red and green algae: Quantification, phylogeny, and relevance for the interpretation of geologic steranes. *Geobiology*, 6, 411–420.
- Koopmans, M. P., Schouten, S., Kohnen, M. E. L., & Damste, J. S. S. (1996).
 Restricted utility of aryl isoprenoids as indicators for photic zone anoxia. Geochimica et Cosmochimica Acta, 60(23), 4873–4876.
- Lu, M., Lu, Y., & Ikejiri, T. (2021). A synthesis of the Devonian widlfire record: Implicatios for paleogeography, fossil flora, and paleoclimate. Palaeogeography, Palaeoclimatology, Palaeoecology, 571, 110321. https://doi.org/10.1016/j.palaeo.2021.110321
- Lu, M., Lu, Y., Ikejiri, T., Hogancamp, N., Sun, Y., Wu, Q., Carroll, R., Çemen, I., & Pashin, J. (2019). Geochemical evidence of first forestation in the southernmost Euramerica from upper Devonian (Famennian) black shales. Scientific Reports, 9, 7581. https://doi.org/10.1038/s41598-019-43993-y
- Lu, M., Lu, Y., Ikejiri, T., Sun, D., Carroll, R., Blair, E. H., Algeoe, T. J., & Sun, Y. (2021). Periodic oceanic euxinia and terrestrial fluxes linked to astronomical forcing during the Late Devonian Frasnian–Famennian mass extinction. *Earth and Planetary Science Letters*, 562, 1–11.
- Malone, T. C., & Newton, A. (2020). The globalization of cultural eutrophication in the Coastal Ocean: Causes and consequences. *Frontiers* in Marine Science, 7, 1–30.
- Marshall, N. L., Love, G. D., Grytsenko, V., & Bekker, A. (2023). Assessing marine communities and carbon cycling that sustained shallowmarine ecosystems on Silurian, reef-rimmed carbonate platforms. *Organic Geochemistry*, 175, 104528. https://doi.org/10.1016/j. orggeochem.2022.104528
- Martinez, A. M., Boyer, D. L., Droser, M. L., Barrie, C., & Love, G. D. (2018). A stable and productive marine microbial community was sustained through the end-Devonian Hangenberg crisis within the Cleveland shale of the Appalachian Basin, United States. *Geobiology*, 17, 27–42.
- Marynowski, L., Kurkiewicz, S., Rakociński, M., & Simoneit, B. R. T. (2011). Effects of weathering on organic matter: I. Changes in molecular composition of extractable organic compounds caused by paleoweathering of a lower carboniferous (Tournaisian) marine black shale. Chemical Geology, 285(1-4), 144-156.
- Marynowski, L., Rakocinski, M., Borcuch, E., Kremer, B., Schubert, B. A., & Jahren, A. H. (2011). Molecular and petrographic indicators of redox conditions and bacterial communities after the F/F mass extinction (Kowala, Holy Cross Mountains, Poland). Palaeogeography Palaeoclimatology Palaeoecology, 306(1-2), 1-14.
- Mastalerz, M., Schimmelmann, A., Drobniak, A., & Chen, Y. (2013).

 Porosity of Devonian and Mississippian New Albany Shale across

- a maturation gradient: Insights from organic petrology, gas adsorption, and mercury intrusion. AAPG Bulletin, 97, 1621–1643.
- Matiatos, I., Wassenaar, L. I., Monteiro, L. R., Venkiteswaran, J. J., Gooddy, D. C., Boeckx, P., Sacchi, E., Yue, F. J., Michalski, G., Alonso-Hernández, C., Biasi, C., Bouchaou, L., Edirisinghe, N. V., Fadhullah, W., Fianko, J. R., García-Moya, A., Kazakis, N., Li, S. L., Luu, M. T. N., ... Welti, N. (2021). Global patterns of nitrate isotope composition in rivers and adjacent aquifers reveal reactive nitrogen cascading. Communications Earth & Environment, 2, 52. https://doi.org/10.1038/s43247-021-00121-x
- Moldowan, J. M., Seifert, W. K., & Gallegos, E. J. (1985). Relationship between petroleum composition and depositional environment of petroleum source rocks. AAPG Bulletin, 69(8), 1255–1268.
- Montoya, J. P. (2008). Nitrogen stable isotopes in marine environments. In D. G. Capone, D. A. Bronk, M. R. Mulholland, & E. J. Carpenter (Eds.), Nitrogen in the marine environment (2nd ed., pp. 1277–1293). Elsevier.
- Naafs, B. D. A., Bianchini, G., Monteiro, F. M., & Sánchez-Baracaldo, P. (2022). The occurrence of 2-methylhopanoids in modern bacteria and the geological record. *Geobiology*, 20, 41–59.
- Over, D. J., Hauf, E., Wallace, J., Chiarello, J., Over, J.-S., Gilleaudeau, G. J., Song, Y., & Algeo, T. J. (2019). Conodont biostratigraphy and magnetic susceptibility of upper Devonian Chattanooga shale, eastern United States: Evidence for episodic deposition and disconformities. Palaeogeography, Palaeoclimatology, Palaeoecology, 524, 137– 149. https://doi.org/https://doi.org/10.1016/j.palaeo.2019.03.017
- Parker, M. S., Mock, T., & Armbrust, E. V. (2008). Genomic insights into marine microalgae. *Annual Review of Genetics*, 42, 619–645.
- Pehr, K., Love, G. D., Kuznetsov, A., Podkovyrov, V., Junium, C. K., Shumlyanskyy, L., Sokur, T., & Bekker, A. (2018). Ediacara biota flourished in oligotrophic and bacterially dominated marine environments across Baltica. *Nature Communications*, 9, 1–10.
- Percival, L. M. E., Marynowski, L., Baudin, F., Goderis, S., Vleeschouwer, D., Rakociński, M., Narkiewicz, K., Corradini, C., Silva, A.-C., & Claeys, P. (2022). Combined nitrogen-isotope and Cyclostratigraphy evidence for temporal and spatial variability in Frasnian-Famennian environmental change. Geochemistry, Geophysics, Geosystems, 23, 1-18
- Percival, L. M. E., Selby, D., Bond, D. P. G., Rakociński, M., Racki, G., Marynowski, L., Adatte, T., Spangenberg, J. E., & Föllmi, K. B. (2019). Pulses of enhanced continental weathering associated with multiple Late Devonian climate perturbations: Evidence from osmium-isotope compositions. *Palaeogeography, Palaeoclimatology, Palaeoecology*, 524, 240–249.
- Peters, K. E., Walters, C. C., & Moldowan, J. M. (2005). The biomarker guide: Volume 2, Biomarkers and isotopes in petroleum systems and earth history. Cambridge University Press.
- Racki, G., Rakocinski, M., Marynowski, L., & Wignall, P. B. (2018). Mercury enrichments and the Frasnian-Famennian biotic crisis: A volcanic trigger proved? *Geology*, 46(6), 543–546.
- Requejo, A. G., Allan, J., Creaney, S., Gray, N. R., & Cole, K. S. (1992). Aryl isoprenoids and diaromatic carotenoids in Paleozoic source rocks and oils from the Western Canada and Williston basins. *Organic Geochemistry*, 19(1–3), 245–264.
- Richoz, S., van de Schootbrugge, B., Pross, J., Puttmann, W., Quan, T. M., Lindstrom, S., Heunisch, C., Fiebig, J., Maquil, R., Schouten, S., Hauzenberger, C. A., & Wignall, P. B. (2012). Hydrogen sulphide poisoning of shallow seas following the end-Triassic extinction. *Nature Geoscience*, 5, 662–667.
- Rohrssen, M., Love, G. D., Fischer, W., Finnegan, S., & Fike, D. A. (2013). Lipid biomarkers record fundamental changes in the microbial community structure of tropical seas during the late Ordovician Hirnantian glaciation. *Geology*, 41(2), 127–130.
- Schwark, L., & Empt, P. (2006). Sterane biomarkers as indicators of palaeozoic algal evolution and extinction events. *Palaeogeography Palaeoclimatology Palaeoecology*, 240(1–2), 225–236.

- Schwark, L., & Frimmel, A. (2004). Chemostratigraphy of the Posidonia black shale, SW-Germany II. Assessment of extent and persistence of photic-zone anoxia using aryl isoprenoid distributions. *Chemical Geology*, 206(3–4), 231–248.
- Sepulveda, J., Wendler, J. E., Summons, R. E., & Hinrichs, K. U. (2009). Rapid resurgence of marine productivity after the cretaceous-Paleogene mass extinction. *Science*, *326*(5949), 129–132.
- Sigman, D. M., Karsh, K. L., & Casciotti, K. L. (2009). Nitrogen isotopes in the ocean. In *Encyclopedia of ocean sciences* (pp. 40–54). Elsevier Ltd.. https://doi.org/10.1016/B978-012374473-9.00632-9
- Smolarek, J., Marynowski, L., Trela, W., Kujawski, P., & Simoneit, B. R. T. (2017). Redox conditions and marine microbial community changes during the end-Ordovician mass extinction event. *Global and Planetary Change*, 149, 105–122.
- Song, Y., Gilleaudeau, G. J., Algeo, T. J., Over, D. J., Lyons, T. W., Anbar, A. D., & Xie, S. C. (2021). Biomarker evidence of algal-microbial community changes linked to redox and salinity variation, upper Devonian Chattanooga shale (Tennessee, USA). Geological Society of America Bulletin, 133(1-2), 409-424.
- Summons, R. E., Jahnke, L. L., Hope, J. M., & Logan, G. A. (1999). 2-methylhopanoids as biomarkers for cyanobacterial oxygenic photosynthesis. *Nature*, 400, 554–557.
- Summons, R. E., & Powell, T. G. (1986). Chlorobiaceae in Palaeozoic seas revealed by biological markers, isotopes and geology. *Nature*, 319, 763–765.
- Summons, R. E., & Powell, T. G. (1987). Identification of aryl isoprenoids in source rocks and crude oils: Biological markers for the green Sulphur bacteria. Geochimica et Cosmochimica Acta, 51(3), 557–566.
- Tappan, H. (1980). Palaeobiology of plant Protists (p. 1028). Freeman.
- Tribovillard, N., Averbuch, O., Devleeschouwer, X., Racki, G., & Riboulleau, A. (2004). Deep-water anoxia over the Frasnian-Famennian boundary (La serre, France): A tectonically induced oceanic anoxic event? *Terra Nova*, 16(5), 288–295. https://doi.org/10.1111/j.1365-3121.2004.00562.x
- Uveges, B. T., Junium, C. K., Boyer, D. L., Cohen, P. A., & Day, J. E. (2019). Biogeochemical controls on black shale deposition during the Frasnian-Famennian biotic crisis in the Illinois and Appalachian basins, USA, inferred from stable isotopes of nitrogen and carbon. *Palaeogeography, Palaeoclimatology, Palaeoecology, 531*, 1–14.
- Volkman, J. K., Barrett, S. M., Blackburn, S. I., Mansour, M. P., Sikes, E. L., & Gelin, F. (1998). Microalgal biomarkers: A review of recent research developments. Organic Geochemistry, 29(5-7), 1163-1179.
- Volkman, J. K., Barrett, S. M., Dunstan, G. A., & Jeffrey, S. W. (1994). Sterol biomarkers for microalgae from the green algal class Prasinophyceae. Organic Geochemistry, 21(12), 1211–1218.
- Wang, X., Zhao, W., Zhang, S., Wang, H., Su, J., Canfeld, D. E., & Hammarlund, E. U. (2018). The aerobic diagenesis of Mesoproterozoic organic matter. *Scientific Reports*, 8(13324), 1-10.
- Welander, P. V., Coleman, M. L., Sessions, A. L., Summons, R. E., & Newman, D. K. (2010). Identification of a methylase required for 2-methylhopanoid production and implications for the interpretation of sedimentary hopanes. Proceedings of the National Academy of Sciences of the United States of America, 107(19), 8537–8542.
- Whalen, M. T., Śliwiński, M. G., Payne, J. H., Day, J. E., Chen, D., & Silva, A.-C. D. (2015). Chemostratigraphy and magnetic susceptibility of the Late Devonian Frasnian-Famennian transition in western Canada and southern China: Implications for carbon and nutrient cycling and mass extinction. Geological Society, London, Special Publications, 414, 37-72.
- Xie, S., Pancost, R. D., Wang, Y., Yang, H., Wignall, P. B., Luo, G., Jia, C., & Chen, L. (2010). Cyanobacterial blooms tied to volcanism during the 5 m.y. Permo-Triassic biotic crisis. *Geology*, 38(5), 447–450.
- Xie, S. C., Algeo, T. J., Zhou, W. F., Ruan, X. Y., Luo, G. M., Huang, J. H., & Yan, J. X. (2017). Contrasting microbial community changes during mass extinctions at the middle/late Permian and Permian/Triassic boundaries. *Earth and Planetary Science Letters*, 460, 180–191.

- Xie, S. C., Pancost, R. D., Huang, J. H., Wignall, P. B., Yu, J. X., Tang, X. Y., Chen, L., Huang, X. Y., & Lai, X. L. (2007). Changes in the global carbon cycle occurred as two episodes during the Permian-Triassic crisis. *Geology*, *35*(12), 1083–1086.
- Xie, S. C., Pancost, R. D., Yin, H. F., Wang, H. M., & Evershed, R. P. (2005). Two episodes of microbial change coupled with Permo/Triassic faunal mass extinction. *Nature*, 434, 494–497.
- Zeng, J., Xu, R., & Gong, Y. (2011). Hydrothermal activities and seawater acidification in the Late Devonian F-F transition: Evidence from geochemistry of rare earth elements. *Science China Earth Sciences*, 54, 540–549.
- Zubkov, M. V. (2014). Faster growth of the major prokaryotic versus eukaryotic ${\rm CO_2}$ fixers in the oligotrophic ocean. *Nature Communications*, 5(3776), 1–6.
- Zundel, M., & Rohmer, M. (1985). Prokaryotic triterpenoids: 1. 3β-Methylhopanoids from Acetobacter species and Methylococcus capsulatus. *European Journal of Biochemistry*, 150, 23–27.

SUPPORTING INFORMATION

Additional supporting information can be found online in the Supporting Information section at the end of this article.

How to cite this article: Chen, J., Hogancamp, N., Lu, M., Ikejiri, T., Malina, N., Ojeda, A., Sun, Y., & Lu, Y. (2023). Lipid biomarkers recording marine microbial community structure changes through the Frasnian-Famennian mass extinction event. *Geobiology*, 00, 1–18. https://doi.org/10.1111/gbi.12568